Chemical Science

ROYAL SOCIETY OF CHEMISTRY

REVIEW

View Article Online
View Journal | View Issue

Cite this: *Chem. Sci.*, 2024, **15**, 12234

Recent advances for enhanced photodynamic therapy: from new mechanisms to innovative strategies

Xia Wang, Jinlei Peng, Chi Meng and Fude Feng *

Photodynamic therapy (PDT) has been developed as a potential cancer treatment approach owing to its non-invasiveness, spatiotemporal control and limited side effects. Currently, great efforts have been made to improve the PDT effect in terms of safety and efficiency. In this review, we highlight recent advances in innovative strategies for enhanced PDT, including (1) the development of novel radicals, (2) design of activatable photosensitizers based on the TME and light, and (3) photocatalytic NADH oxidation to damage the mitochondrial electron transport chain. Additionally, the new mechanisms for PDT are also presented as an inspiration for the design of novel PSs. Finally, we discuss the current challenges and future prospects in the clinical practice of these innovative strategies. It is hoped that this review will provide a new angle for understanding the relationship between the intratumoural redox environment and PDT mechanisms, and new ideas for the future development of smart PDT systems.

Received 30th December 2023
Accepted 11th July 2024

DOI: 10.1039/d3sc07006a

rsc.li/chemical-science

1. Introduction

Cancer is currently one of the most devastating diseases in the world, presenting a serious threat to human health due to its high morbidity and mortality.[1] To date, the classical clinical diagnosis and treatment methods including surgery, chemotherapy and radiotherapy have made great progress. However, some deficiencies still exist in these treatments such as invasive operations, drug resistance, a high recurrence rate, severe systemic toxicity and long-term adverse effects.[2–4] Thus, novel therapies with few side effects and excellent antitumour activities are highly needed. Among them, photodynamic therapy (PDT) has drawn increasing interest due to its non-invasiveness, spatiotemporal control, limited side effects and low risk in generating drug resistance.[5,6] PDT usually requires three basic components: photosensitizers (PSs), light and oxygen (O_2). In the presence of light and O_2, the activated PSs can produce toxic reactive oxygen species (ROS) to induce tumour cell death through necrosis, apoptosis, autophagy or ferroptosis.[7] As the half-life is usually very short (<40 ns), ROS exert a local effect within a rather short distance (<20 nm).[8,9] As a ROS sensitive crucial subcellular organelle, the mitochondrion is an important component of the apoptosis pathway of cancer cells.[10–12] Accordingly, the development of mitochondria-targeting PSs has become a promising strategy for efficient PDT.

The mechanisms of PDT are generally divided into two categories according to the photophysical and photochemical basis (Fig. 1).[13,14] Under light irradiation, the PS at the ground singlet state (S_0) is excited to a singlet state (S_1), and subsequently populated into a long-lived triplet state (T_1) through intersystem crossing (ISC) and internal conversion (IC) steps. For type I PDT, triplet PSs react directly with the intracellular substances through a hydrogen or electron transfer process to produce reactive free radicals, which further react with O_2 or other substances to generate ROS such as hydrogen peroxide (H_2O_2), the hydroxyl radical ($^{\bullet}OH$) and superoxide anion ($O_2^{\bullet-}$).[15] The effect of type I PSs is less dependent on the O_2 concentration, and therefore type I PSs are preferred for PDT, particularly when O_2 supply is insufficient. However, the majority of reported PDT systems are based on type II PSs.[16,17] For type II PSs, the triplet excited energy is transferred to O_2, generating highly cytotoxic singlet oxygen ($^1O_2$).[18,19] The effect of

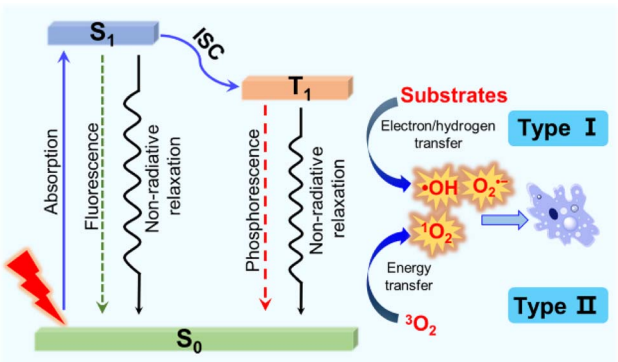

Fig. 1 The photosensitization process and photochemical reaction mechanisms of type I and type II PDT.

MOE Key Laboratory of High Performance Polymer Materials and Technology, Department of Polymer Science & Engineering, School of Chemistry & Chemical Engineering, Nanjing University, Nanjing 210023, China. E-mail: fengfd@nju.edu.cn

O_2-dependent type II PSs is limited in the hypoxic tumour microenvironment (TME).

Three generations of PSs have been developed for anticancer PDT so far and a variety of PSs (*e.g.*, porphyrin, chlorin, BODIPY) have been commercialized or used in clinical trials.[17,20,21] The first generation of PSs is based on a mixture of porphyrin complexes, including hematoporphyrin derivative (HpD), dihematoporphyrin ether (DHE), and Photofrin porfimer sodium. However, low efficiency and poor tissue penetration limit clinical practice in PDT.[5] The second generation of PSs in accurate structures (*e.g.*, 5-aminolevulinic acid (5-ALA), phthalocyanines, hypericin, metalloporphyrins) have been developed, but suffer from poor solubility and tumour targeting issues.[22] To improve the selectivity to tumours and reduce the damage to normal tissues, the third generation of PSs are equipped with cancer-targeting ligands, including folic acid, peptides, antibody, and aptamer.[23] Nevertheless, PDT still faces some challenges that hinder its widespread clinical application: (1) PDT requires light that reaches the target area, so its therapeutic effect is quite restricted to tumours in the skin or areas adjacent to the organs.[24,25] (2) The penetration depth of light in tumour tissues strongly depends on its wavelength. However, as most PSs weakly absorb near-infrared (NIR) light, tissue penetration is limited significantly in the use of high-energy short-wavelength excitation (UV, blue, or green light).[16,17] (3) Due to the excessive proliferation of cancer cells and insufficient blood supply, the O_2 concentration in solid tumours is severely abnormal,[26,27] resulting in the significant decrease of PDT efficacy.

In recent years, great efforts have been made to enhance the PDT effect. The strategies mainly focus on the reconstruction of the TME to alleviate tumour hypoxia,[28–31] development of novel type I PSs with tumour targeting capability and longer absorption wavelength,[32–34] and combination of PDT with other treatments.[35–37] Advances in PDT have been introduced comprehensively in previous reviews.[23,38–40] Herein, we collectively review the state-of-the-art development of recent PDT strategies that primarily aim at mitochondria and a little bit at other organelles (*e.g.*, lysosome and endoplasmic reticulum) and provide prospects for future high-performance PDT systems that rely on the endogenous redox-environment. The innovative strategies are roughly classified into three categories: (1) the development of novel radicals including the hydrogen radical ($H^{\bullet}$) and carbon radical ($C^{\bullet}$), (2) activatable PSs based on the TME and light, and (3) photocatalytic oxidation of 1,4-dihydronicotinamide adenine dinucleotide (NADH) (Fig. 2). These methods involve new mechanisms of PDT (*e.g.*, photoredox catalysis) and can be carried out in an O_2-independent manner to achieve PDT in the hypoxic TME. However, to promote clinical use of the new mechanisms, developing long-wavelength NIR PSs to increase tissue penetration depth is of great importance. In addition, tumour-targeting therapy needs to be considered to avoid nonspecific damage to surrounding healthy tissues. We hope this review will inspire more significant design of PSs based on new mechanisms for precision cancer therapy.

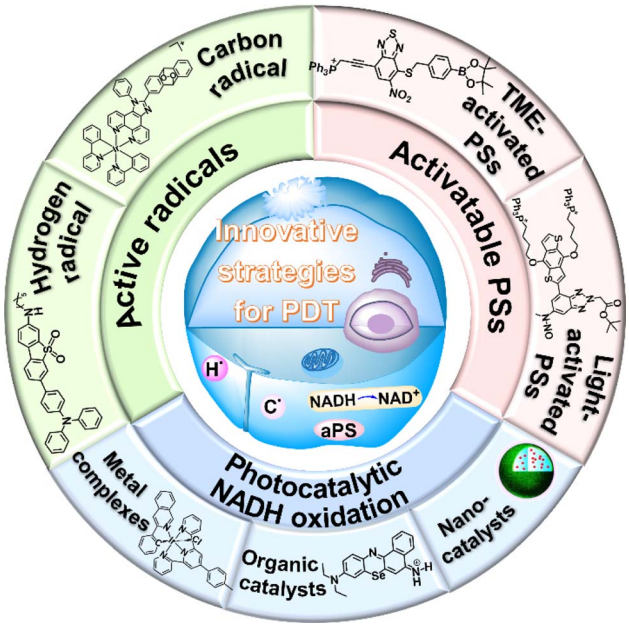

Fig. 2 The innovative strategies for enhanced PDT.

2. Novel radical-based PDT

Free radicals have attracted increasing attention because they can fight against different types of tumours without causing drug resistance.[41] The generation of toxic ROS, which is largely dependent on the concentration of O_2 and H_2O_2, is inadequate on the hypoxic tumour.[42] It is crucial to explore more free radicals (*e.g.*, chlorine radicals,[43] carbon radicals[44] and hydrogen radicals[45,46]) independent of O_2 and H_2O_2 in PDT. In this section, research on $H^{\bullet}$- and $C^{\bullet}$-based PDT is discussed in detail.

2.1 Hydrogen radical

As a reactive hydrogen species (RHS), $H^{\bullet}$ can be generated *via* ultrasound and ionizing radiation and is reactive to a spectrum of species such as radicals, high valence metals and unsaturated bonds.[47,48] Bradley *et al.* reported that water radiolysis by γ/X-ray irradiation could mediate the activation of a cancer prodrug with the azide group by $H^{\bullet}$.[49] Studer *et al.* achieved water activation with a photocatalytic phosphine-mediated radical process under 455 nm light irradiation.[50] The generated PR_3–H_2O radical cation was deprotonated to form a neutral PR_3–OH radical intermediate followed by a heterolytic O–H bond cleavage. The PR_3–OH radical behaved as a 'free' H atom and was used to reduce π systems. $H^{\bullet}$ is a two-sided modulator due to its unique redox properties. It is a pro-oxidant due to it scavenging O_2 ($k = 2.1 \times 10^{10}$ M^{-1} s^{-1}) into the hydroperoxyl radical ($HO_2^{\cdot}$) or $O_2^{\bullet-}$ under aerobic conditions, and also acts as a powerful reductant in an anaerobic environment.[46] To date, $H^{\bullet}$-based therapy has been scarcely investigated.[45,46,51]

In 2021, we reported a benzotriazole-cored activatable PS (aPS), termed DANO, that was flanked by two triphenylphosphonium (TPP) units to target mitochondria and equipped with

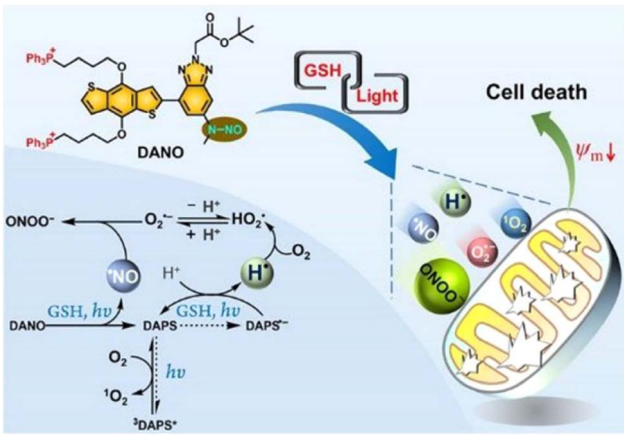

Fig. 3 Schematic illustration of the photogeneration of H•, $O_2^{\bullet-}$/$HO_2^{\bullet}$, •NO, $ONOO^-$, and $^1O_2$ upon coactivation of DANO with GSH and light. Reproduced with permission from ref. 45. Copyright 2021 American Chemical Society.

an *N*-nitrosamine moiety as a donor of the nitric oxide radical (•NO) as well as photocaging functionality. In the co-existence of reduced glutathione (GSH) and visible light, DANO was converted to the photoactive form (DAPS), with concomitant liberation of •NO that was initiated by the homolytic N–N bond scission at the *N*-nitrosamine moiety (Fig. 3).[45] Different from the general PDT process, H• was detected by the electron spin resonance (ESR) technique and was responsible for the production of $O_2^{\bullet-}$. Free radical recombination between •NO and $O_2^{\bullet-}$ led to immediate formation of peroxynitrite ($ONOO^-$), a reactive nitrogen species (RNS) with greatly increased cytotoxicity relative to •NO and $O_2^{\bullet-}$. The PDT effect on HeLa cells under both normoxia and hypoxia was maximized by the simultaneous production of multiple reactive species that originated from H• and •NO cascade reactions upon photoactivation of DANO in the GSH-abundant mitochondria. Efficient two-photon excited PDT with DANO was also achieved by using an 800 nm two-photon laser, which showed the potential of DANO in precise cancer phototherapy.

To look into the mechanism of H• production and its role in the PDT process, our group designed an efficient photochemical H• generator based on a donor–acceptor type PS (termed TAF) that consisted of triphenylamine and hexylamine-substituted dibenzothiophene sulfone units (Fig. 4a).[46] Mechanically, the triplet excited TAF is reducible by GSH to form $TAF^{\bullet-}$, which is protonated and returned to the original state with concomitant release of H• (Fig. 4b). The key intermediate radical ($TAFH^{\bullet}$) was successfully captured by 2,2,6,6-tetramethyl-1-piperidinyloxy (TEMPO) and the adduct product was identified by high resolution mass spectroscopy (HRMS). The role of H• in PDT is two-fold. One is the H•-promoted oxidative effect *via* scavenging of O_2 to produce $O_2^{\bullet-}$ that amplifies the oxidative stress under normoxia, which leads to ferroptosis–apoptosis of tumour cells. The other one is associated with the strong chemical reducing properties of H• in causing tumour cell apoptosis and breaking the traditional PDT barrier of extreme hypoxia. In the *in vitro* study, TAF showed a very high photocytotoxicity index (PI) on HeLa and A549 cells under normoxia and hypoxia. This work establishes a GSH-driven and H•-based phototherapy and solves the self-limiting hypoxia dilemma of PDT.

2.2 Carbon radical

C• can be generated in the absence of O_2, presenting significant potential as a candidate cytotoxic species for PDT. Tirapazamine (TPZ), as a hypoxia-activable prodrug (HAP), can be bioreduced to an alkyl radical (and hydroxyl radical) in the TME, attracting hydrogen from DNA strands and consequently causing DNA cleavage.[52] The water-soluble 2,2-azobis[2-(2-imidazolin-2-yl)propane] dihydrochloride (AIPH) is chemically unstable and is often used as an alkyl radical precursor.[53] As an azo compound, AIPH rapidly decomposes to generate cytotoxic alkyl radicals upon exposure to light or heat.[54–56]

Lee *et al.* constructed a smart nanoformulation system consisting of gold nanorods (GNRs) and AIPH in a poly(lactic-*co*-glycolic acid) (PLGA) matrix, which could form and release C• in response to external NIR light irradiation (Fig. 5a).[57] The use of

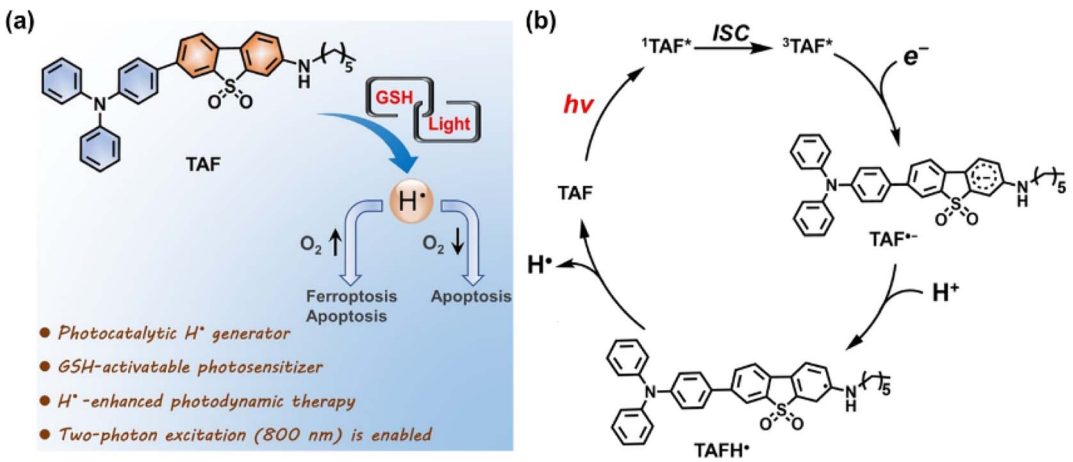

Fig. 4 (a) Schematic presentation of GSH-driven H• photogeneration for PDT. (b) Proposed mechanism for photocatalytic H• generation. Reproduced with permission from ref. 46. Copyright 2022 Wiley-VCH.

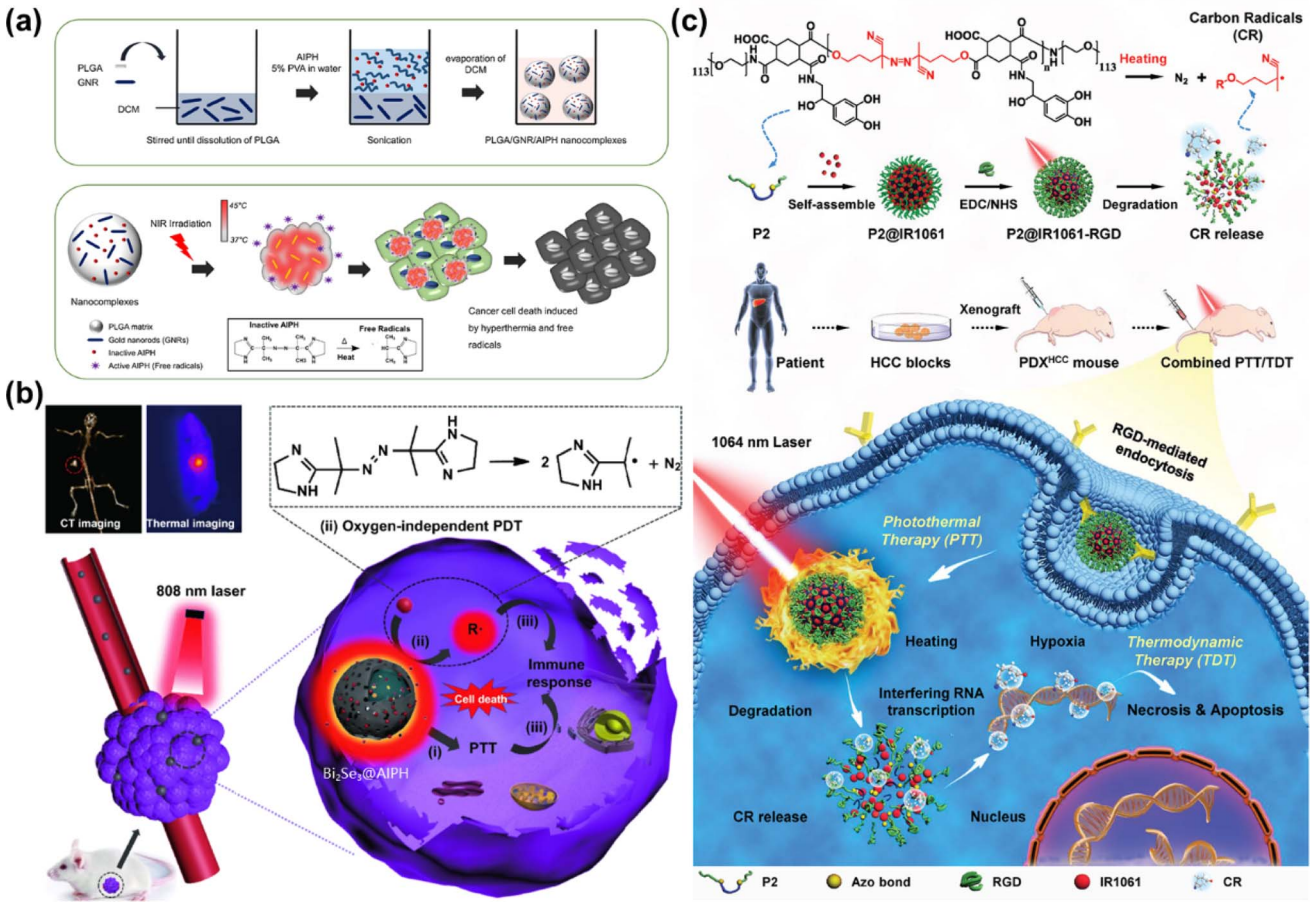

Fig. 5 (a) Synthesis of poly(lactic-*co*-glycolic acid) (PLGA)/gold nanorod (GNR)/2,2′-azobis[2-(2-imidazolin-2-yl)propane] dihydrochloride (AIPH) nanocomplexes and schematic illustration of the PLGA/GNR/AIPH nanocomplexes allowing near-infrared (NIR) induced heat and free radical generation for efficient dual cancer treatment. Reproduced with permission from ref. 57. Copyright 2018 Elsevier B.V. (b) Theranostic process of Bi_2Se_3@AIPH for CT and thermal imaging-guided cascaded photothermal and oxygen-independent photodynamic therapy along with immune response. Reproduced with permission from ref. 58. Copyright 2019 Springer Nature. (c) Preparation of P2@IR1061-RGD for combined PTT and TDT in a NIR II window (1000–1700 nm) of the PDX^{HCC} mouse model. Reproduced with permission from ref. 59. Copyright 2021 Wiley-VCH.

the PLGA polymer matrix allowed for a high loading capacity of AIPH and protection from burst release. *In vitro* studies demonstrated the nanocomplexes can eradicate CT26 colon cancer cells effectively. In 2019, Yuan *et al.* prepared Bi_2Se_3@AIPH through encapsulating AIPH and a phase transition material (lauric acid) in hollow bismuth selenide nanoparticles (Bi_2Se_3 NPs) (Fig. 5b).[58] When circulating in the blood, AIPH was encapsulated without leakage to avoid side effects. In the tumour tissues of mice, Bi_2Se_3@AIPH presented a strong photothermal (PTT) effect after 808 nm laser irradiation, accompanied by the release of AIPH to produce C$^{\bullet}$, leading to GSH depletion and an amplified immune response, showing a tumour growth inhibition rate of 99.6%.

Light in the NIR II window (1000–1700 nm) exhibits deep tissue penetration (>1 cm) because of the reduced tissue absorption and scattering, suitable for treatment of deep tumours. Liu *et al.* reported a degradable nano-system (P2@IR1061-RGD NPs) formed *via* self-assembly between an amphiphilic thermolabile azo-containing polymer (P2) and a NIR II photothermal dye IR1061 to achieve safe and efficient cancer therapy (Fig. 5c).[59] P2@IR1061-RGD NPs were degraded by the photothermal effect of IR1061 with robust C$^{\bullet}$ generation once irradiated at 1064 nm, thereby interfering with RNA transcription, as well as inducing cancer cell necrosis or apoptosis even in the hypoxic tumour microenvironment. The nano-system displayed excellent tumour inhibition on a 4T1 breast cancer model as well as a patient-derived xenograft model of hepatocellular carcinoma (PDX^{HCC}), with inhibition rates up to 97% and 100%, respectively, which is promising for clinical therapy on deep tissue hypoxic tumours without serious systemic toxicity.

In 2020, Chao *et al.* reported an iridium(III) anthraquinone complex (Ir_4) as a mitochondria-targeting C$^{\bullet}$ initiator (Fig. 6a).[60] The anthraquinone moiety was used as a light-activated C$^{\bullet}$ initiator as well as a luminescence quencher. In the hypoxic tumour, Ir4 was reduced to anthracene diol (Ir4-red) by the overexpressed reductase, which led to turn-on response of the two-photon excited luminescence. Ir4-red could generate C$^{\bullet}$ under two-photon excitation (730 nm) and exhibit dual functions in bioimaging and therapy. In the *in vitro* (A549 3D

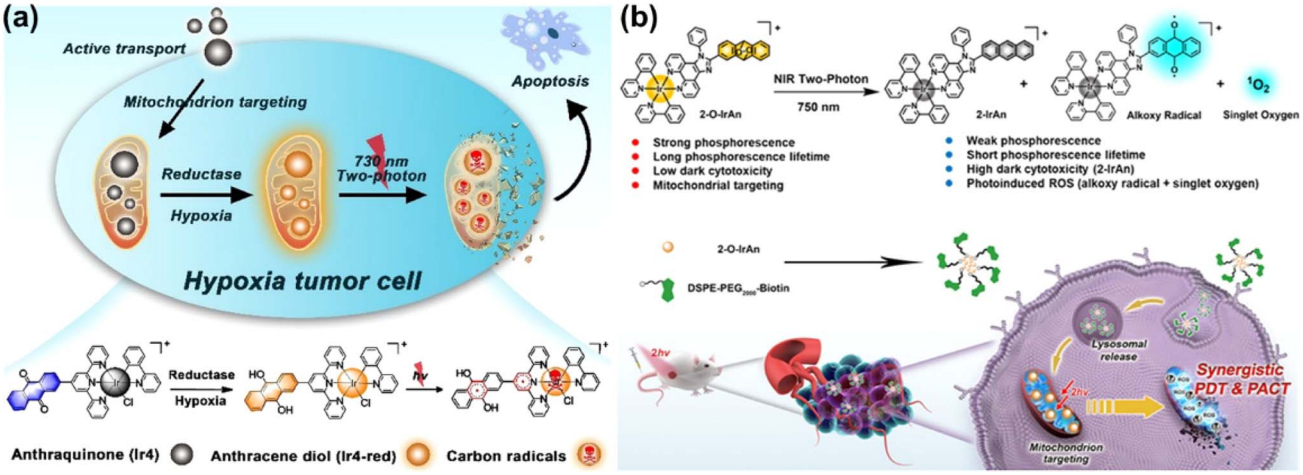

Fig. 6 (a) Proposed schematic illustration of the PDT mechanism of the Ir4 complex. Reproduced with permission from ref. 60. Copyright 2020 Wiley-VCH. (b) Schematic illustration of the mechanism of the action of the Ir(III) complex by PDT/PACT. Reproduced with permission from ref. 61. Copyright 2022 American Chemical Society.

multicellular tumour spheroids) and *in vivo* (male nude mice bearing A549 xenografted tumours) studies, Ir4 presented an outstanding PDT effect for its strong C˙ generating capability. To improve the phototoxic effect and promote clinical application of the metal complex, Chao's group further designed a mitochondria-localized iridium(III) endoperoxide prodrug (2-O–IrAn), which could synergistically release a highly cytotoxic iridium(III) complex (2-IrAn), $^1O_2$, and an alkoxy radical upon two-photon irradiation (750 nm) (Fig. 6b).[61] Then 2-O–IrAn was encapsulated into a biotin-functionalized polymer to obtain DSPE-PEG-Biotin@2-O–IrAn NPs in order to provide cancer selectivity and improve the pharmacological properties. Under two-photon irradiation (750 nm, 50 mW, 300 s), the generated nanoparticles nearly fully eradicated the tumour inside A549 tumour-bearing mice within a single treatment *via* synergistic PDT/photoactivated chemotherapy (PACT).

3. Activatable PSs for PDT

The ability of PSs to generate ROS selectively at the tumour site remains one of the important factors in maximizing the therapeutic effect while minimizing damage to normal cells. However, most PSs are in the "always on" stage, which poses a risk of damage to normal cells during the PDT process.[62–64] This issue is alleviated by using activable PSs (aPSs) as PS precursors. The aPSs functionalized with caged groups are originally inactive and their activity can be precisely activated by tumour-specific endogenous stimuli (pH, enzyme, redox, *etc.*) or exogenous stimuli (ultrasound, temperature, light, *etc.*),[65–67] which contribute to improving treatment efficiency and reducing side effects on healthy tissues. In this section, we will highlight the relevant reports of activatable PDT systems and hope to provide an inspiration for the design of PSs.

3.1 TME-activated PSs

TME refers to the local steady-state environment composed of tumour cells, stromal cells, and the extracellular matrix during tumour growth. The TME provides the necessary material basis for tumour occurrence, development, invasion, and metastasis.[68,69] In the TME, due to the slow blood flow of oxygen to tumour cells and the rapid cell proliferation, tumours present the hypoxic state.[70] In addition, the TME also exhibits the features of lower intercellular pH and higher intracellular GSH and H_2O_2 concentration.[71,72] These unique characteristics of the TME distinguish it from the corresponding normal tissues, thereby helping the design of TME-activated PSs.

3.1.1 Hypoxia-activated PSs. Hypoxia, as a hallmark of the TME, can cause two key intracellular responses. One is stabilization of hypoxia inducible factor-1 (HIF-1), and the other is the imbalance of the cellular redox state, leading to the high expression of reductase (azoreductase, nitroreductase, *etc.*), which makes reductase an endogenous biomarker for cellular hypoxia.[73] Until now, a series of hypoxia-activated bioreductive prodrugs (*e.g.*, tirapazamine (TPZ), banoxantrone (AQ4N), apaziquone (EO9))[74] and prodrugs caged with hypoxia-sensitive groups (such as the azo bond) have been developed for cancer therapy.

The real-time monitoring of the drug release induced by hypoxia can obtain feedback on the treatment process in time. In 2022, Kim *et al.* engineered a compound (DHQ-Cl-Azo) with hypoxia-responsive chemotherapy and PDT functionalities for the cooperative treatment of solid tumours (Fig. 7a).[75] DHQ-Cl-Azo was obtained through a covalent connection using a hypoxia-sensitive azo bond (–N=N–) bridge between a NIR rhodol-based fluorophore (DHQ-Cl) and the nitrogen mustard drug. In the hypoxic TME, the azo bond of DHQ-Cl-Azo was reduced by azoreductase, leading to the release of the nitrogen mustard for chemotherapy and DHQ-Cl for PDT and diagnosis. DHQ-Cl-Azo helped to eliminate tumour cells in the surface layer during PDT and was beneficial for eradicating hypoxic tumour cells in the tumour center during activation of chemotherapy, thereby maximizing the anti-cancer effect on 4T1 tumour-bearing BALB/c mice.

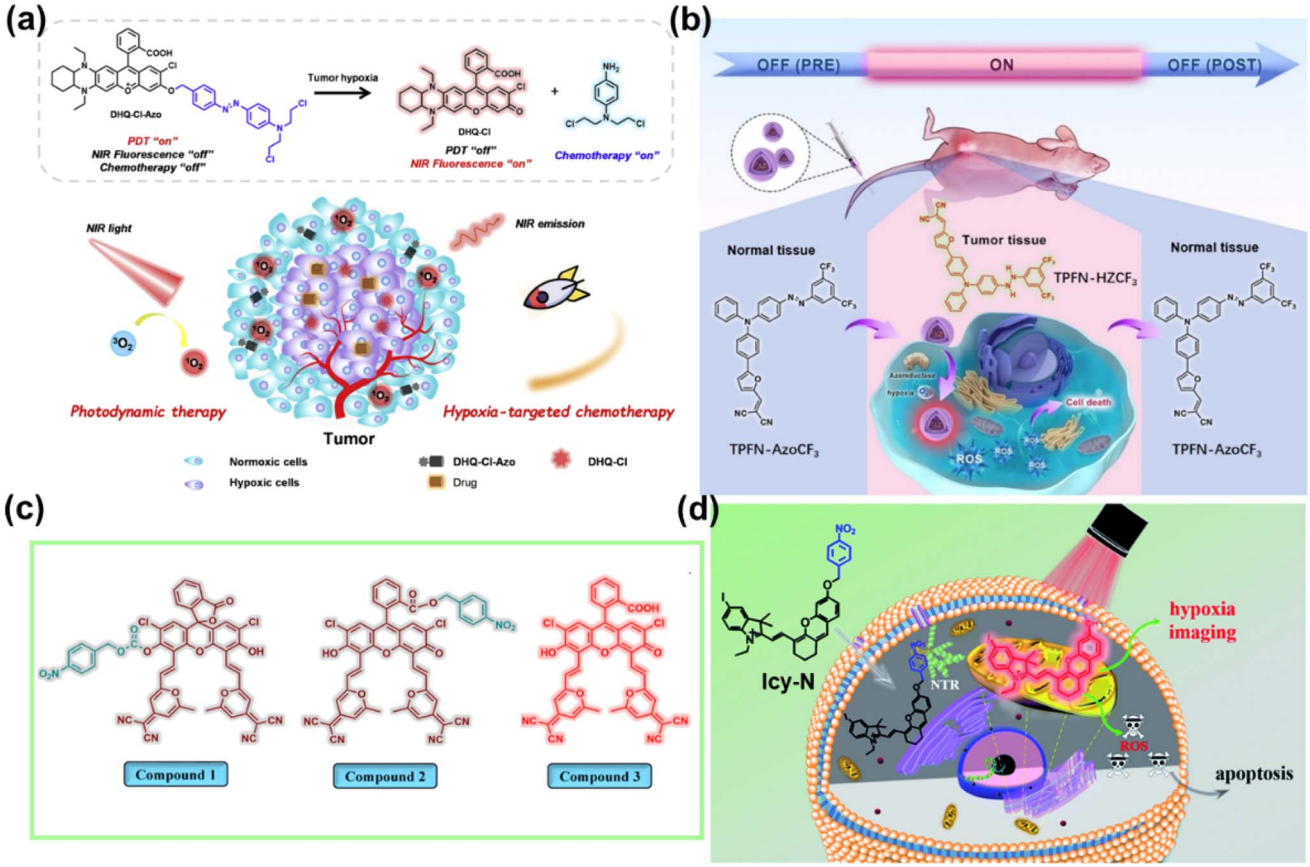

Fig. 7 (a) Principle of DHQ-Cl-Azo for PDT and chemotherapy. Reproduced with permission from ref. 75. Copyright 2022 Elsevier Inc. (b) A reversible hypoxia–normoxia responsive type I photosensitizer for PDT. Reproduced with permission from ref. 76. Copyright 2023 Wiley-VCH. (c) Molecular structures of compounds 1–3. Reproduced with permission from ref. 77. Copyright 2019 American Chemical Society. (d) ICy-N for hypoxia imaging and cancer therapy. Reproduced with permission from ref. 78. Copyright 2019 The Royal Society of Chemistry.

The off–on PSs retain their phototoxic form even after treatment. Thus, it is crucial to alleviate the side effects associated with post-treatment of PDT. Liu *et al.* reported an on-demand switchable type I PS (TPFN–AzoCF$_3$) that was activated only in the TME (Fig. 7b) and inactivated pre and post PDT.[76] TPFN–AzoCF$_3$ was composed of a type I PS (TPFN) and a hypoxia–normoxia cycling responsive group (AzoCF$_3$). The arylazo group served as an off–on–off trigger that reversibly transformed into a hydrazine group depending on hypoxia–normoxia conditions. TPFN–AzoCF$_3$ was converted into TPFN–HZCF$_3$ in hypoxic environments, resulting in PS turn-on and effective ROS generation, but remained non-toxic in normal tissues pre or post PDT, which contributed to minimal side effects. TPFN–AzoCF$_3$ revealed a satisfactory antitumour effect on a xenografted subcutaneous model of HeLa tumours *in vivo* with safe pre- and post-treatment for PDT.

Overexpressed nitroreductase (NTR) inside hypoxic tumour tissues is another widely studied reductase. Peng *et al.* developed fluorescein derivatives as smart PSs activated by NTR with thermally activated delayed fluorescence (TADF).[77] They designed compound 1 and compound 2 with fluorescence and PDT efficiency in the "off" state. In the presence of NTR, both compounds containing a nitrobenzyl substituent were transformed into compound 3 *via* intramolecular photoinduced electron transfer (PET) (Fig. 7c). The faster response observed with compound 2 was ascribed to the higher affinity between compound 2 and NTR. Further, efficient PDT on compound 2-treated HeLa cells and HeLa tumour-bearing mice was achieved under 590 nm LED light irradiation. A similar strategy was applied to the iodized hemicyanine dye conjugated with a nitrobenzyl substituent, which could be efficiently used for tumour hypoxia imaging (710 nm) and PDT in 4T1 cells and 4T1 tumour bearing BALB/c mice under 660 nm light irradiation (Fig. 7d).[78]

3.1.2 pH-activated PSs. Tumour cells usually rely on glycolysis for energy production, namely the Warburg effect, leading to the generation of large amounts of lactate as a by-product and a weakly acidified TME relative to the normal tissues and blood.[79] The extracellular pH in the TME varies between 5.8 and 7.2, while the pH in lysosomes or endosomes is approximately 5.5,[80] which provides a suitable endogenous stimulus for the activation of prodrugs and promotes the extensive development of pH-activated PSs in PDT.

In 2022, Yoon *et al.* constructed an acid-responsive nanoporphyrin (PN$_3$-NP) based on the self-assembly of a water-soluble porphyrin derivative (PN$_3$).[81] PN$_3$-NP could transform from nanoparticles into dot-like nanospheres due to the reconstruction of the substructure in the acidic environment. Simultaneously, NIR fluorescence monitoring and synergistic

PDT and PTT effects of PN_3-NP were also triggered in biofilms, achieving accurate theranostics without damage to normal tissues. Siegwart *et al.* designed an iodinated, water-soluble NIR BODIPY-based PS that could be activated by leveraging tumour-specific pH for image-guided and efficient PDT against cancer *in vivo* (Fig. 8a).[82] At the physiological pH, the $^1O_2$ release was "turned off" *via* the PET process, while the quenching process was inhibited and the $^1O_2$ release was "turned on" upon the protonation of the amino groups at acidic pH, inducing cell death *via* apoptosis in a cancer-selective manner. The PS presented excellent photocytotoxicity on different cancer lines *in vitro*, and significant anticancer efficacy on athymic nude mice bearing subcutaneous MDA-MB-231 xenograft tumours after treatment with a 600–700 nm laser.

Moreover, the acylamide bond was responsive to the acidified TME as well, which is favorable for designing pH-responsive prodrugs. In 2023, Chen *et al.* utilized acylamide bonds as a linker to synthesize TPZ-functionalized poly(ethylene glycol) (PEG–TPZ), and prepared a multi-responsive nanoplatform for phototherapy-enhanced chemotherapy based on PEG–TPZ encapsulated semiconducting polymer TDPP (Fig. 8b).[83] The nanoplatform could release TPZ by the hydrolysis of the acylamide bond. Efficient ROS and photothermal conversion were triggered by laser irradiation, resulting in the consumption of cellular oxygen as well as damage to the blood vessels. The aggravated hypoxia contributed to the activation of TPZ for chemotherapy, which in turn enhanced therapeutic efficacy. TDPP@PEG–TPZ NPs showed a great treatment effect in *in vitro* (143B cells) and *in vivo* (143B tumour-bearing mice) experiments.

Reversibly switchable ISC is crucial to deactivate photosensitization when PS is transferred or metabolized away from the pathological region. The availability of conjugated backbone twist (CBT)-enhanced ISC offers a unique opportunity for the

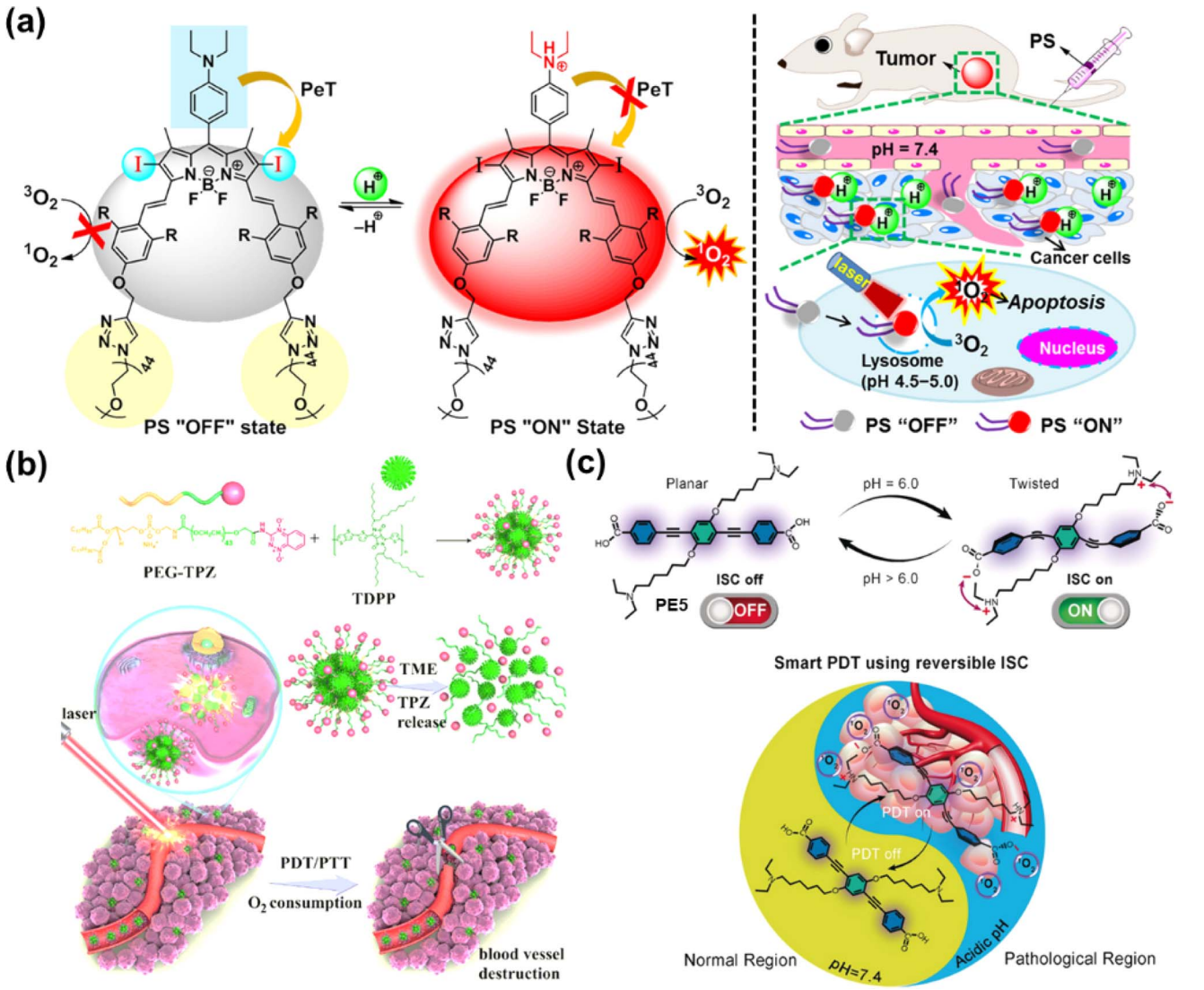

Fig. 8 (a) The pH-activatable BODIPY derivative for $^1O_2$ generation and PDT. Reproduced with permission from ref. 82. Copyright 2018 American Chemical Society. (b) Illustration of the TDPP@PEG–TPZ nanoformulation for phototherapy-enhanced chemotherapy. Reproduced with permission from ref. 83. Copyright 2023 The Royal Society of Chemistry. (c) Reversible switching of ISC and potential application in PDT. Reproduced with permission from ref. 84. Copyright 2019 Wiley-VCH.

reversible on–off switch of PSs. Prasad *et al.* presented reversible switching of ISC using PE5 through the pH-responsive CBT (Fig. 8c).[84] At physiological pH (pH 7.4), PE5 existed mainly in anionic form with no electrostatic interactions to drive the twisted geometry, showing "ISC off". However, PE5 transformed to a zwitterionic form at pH 6.0 and formation of the CBT conformation occurred, which led to "ISC on" and an efficient PDT effect. In the *in vitro* study, PE5 exhibited outstanding selectivity for tumour cells.

3.1.3 Enzyme-activated PSs. Cancer cells often overexpress a variety of enzymes such as prostate-specific membrane antigen (PSMA), hyaluronidases (HAase), esterase, matrix metalloproteins (MMPs), and phospholipases, for the rapid growth and metathesis of tumours.[80,85] Thus, the difference in the level of enzyme expression has been exploited widely in designing enzyme-activated PSs with the targeting capability on tumour areas.

Compared to traditional PSs with the aggregation-caused quenching (ACQ) effect, aggregation-induced emission (AIE) molecular PSs can restrict intermolecular π–π stacking and intramolecular motions when aggregated, which will be conducive to improving fluorescence imaging and phototherapy.[86,87] To develop novel PSs with higher photosensitive properties and specific target response ability, Li *et al.* synthesized an enzyme-activatable AIE molecular photosensitizer (TPE–TThPy) using the conjugation of tetraphenylethylene

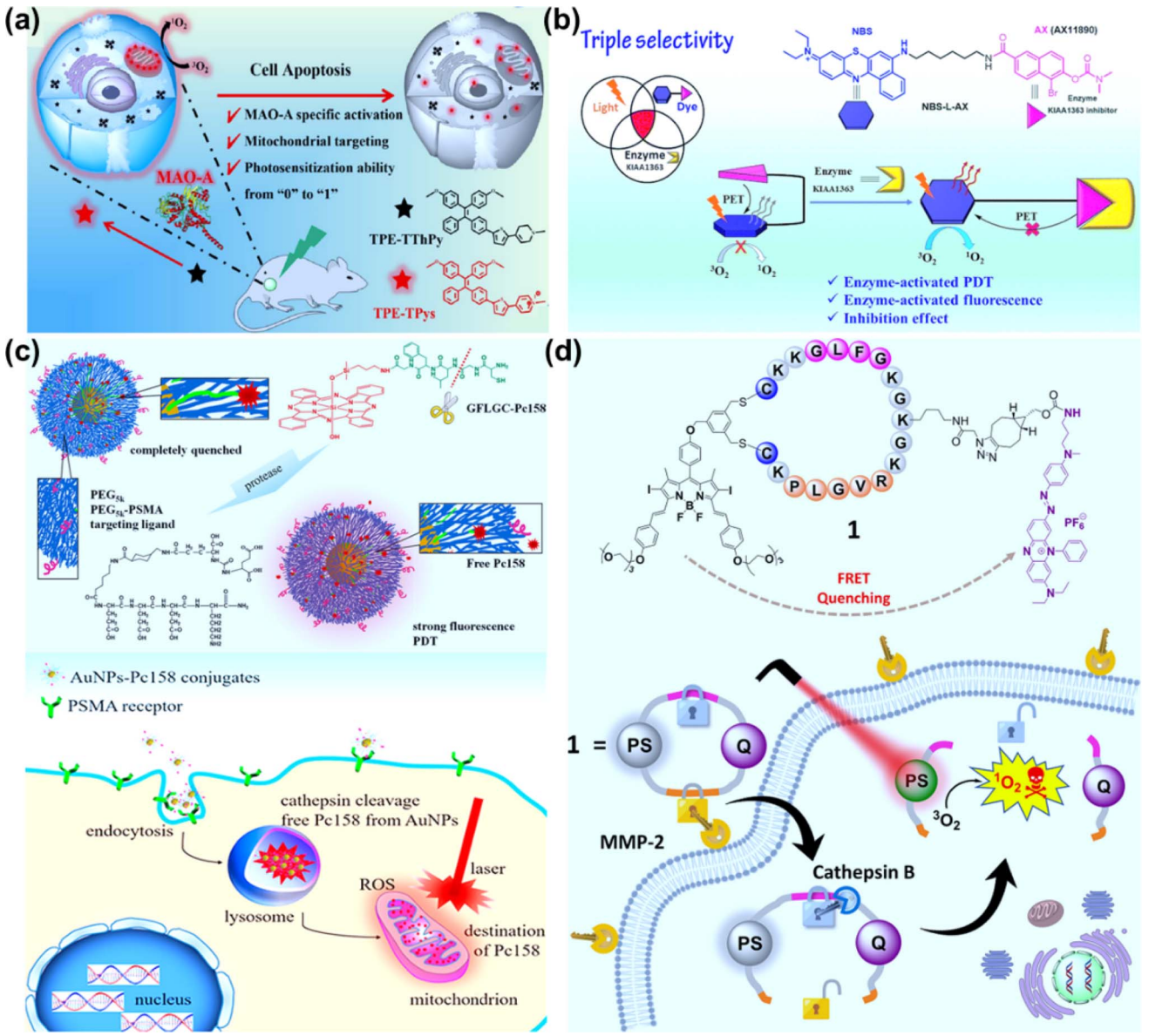

Fig. 9 (a) TPE–TThPy as a mitochondria-targeting photosensitizer for MAO-A-activatable PDT. Reproduced with permission from ref. 88. Copyright 2022 Wiley-VCH. (b) Enzyme KIAA1363-activated mechanism for NBS-L-AX based PDT. Reproduced with permission from ref. 90. Copyright 2023 The Royal Society of Chemistry. (c) Cathepsin-activated AuNPs–Pc158 conjugates for selective PDT. Reproduced with permission from ref. 94. Copyright 2020 American Chemical Society. (d) Molecular structure of the double-locked PMB 1 and its dual-enzyme-unlocked mechanism. Reproduced with permission from ref. 95. Copyright 2023 American Chemical Society.

(TPE) and tetrahydropyridine (ThPy) with thiophene (T) as the π-bridge (Fig. 9a).[88] The TPE–TThPy molecule was responsive to monoamine oxidase (MAOs), a kind of flavinase overexpressed in tumour cells, which converted ThPy to methylpyridine salts (Pys). The cationic TPE–TPys showed mitochondrial targeting properties and ROS photogeneration capability. *In vivo* studies revealed a strong inhibitory effect of photoexcited TPE–TThPy on nude BALB/c mice bearing a subcutaneous SH-SY5Y xenograft with high MAO-A expression.

AX11890 has strong binding affinity toward the KIAA1363 enzyme and is an inhibitor of overexpressed KIAA1363 enzyme in breast cancers.[89] Foley *et al.* constructed NBS-L-AX by attaching a benzo[*a*]phenothiazine moiety with a short linear alkyl chain (NBS-L) to enzyme targeting agent AX11890 (Fig. 9b).[90] In normal tissues, NBS-L-AX exhibited a compact sandwiched conformation due to the strong π–π interaction between the NBS-L and AX11890 moieties, which favored a PET process from AX11890 to NBS-L and quenched the fluorescence and PDT activity of NBS-L. In breast cancer cells, when NBS-L-AX was in contact with the KIAA1363, KIAA1363 bound to the AX11890 segment and concomitantly unraveled the sandwiched NBS-L-AX molecule to form a fully extended linear conformation, switching on the fluorescence and PDT activities of the NBS-L segment. In the *in vitro* experiments, higher photocytotoxicity to KIAA1363-positive MCF-7 cells than KIAA1363-negative HUVEC cells was observed. In the *in vivo* experiments, NBS-L-AX presented good selectivity on the 4T1 tumour-bearing mice model under 635 nm laser irradiation (100 mW cm^{-2}, 20 min).

The fact that extracellular adenosine triphosphate (ATP) is overexpressed in the tumour tissues has been applied in fabricating nanodrugs for tumour-targeting delivery. Schanze *et al.* reported metal-free helical nanofibers formed in aqueous solution using the co-assembly of a cationic porphyrin and ATP for PDT.[91] The porphyrin–ATP assembly was delivered to the tumour site through whole-body blood circulation and was stabilized *via* overexpressed extracellular ATP within tumour tissues. The release of porphyrin upon biodegradation of ATP by intracellular phosphatases gave rise to tumour-selective PDT.

Cathepsins are highly abundant within intracellular endolysosomal vesicles in cancer cells. Upregulated cathepsin activity is strongly associated with tumour invasion and metastasis,[92,93] which has made cathepsin an excellent tumour-associated biomarker to "turn on" PSs for precise PDT. Basilion *et al.* designed PSMA-targeting cathepsin activatable AuNPs for treating prostate cancer.[94] Silicon phthalocyanine (Pc158) was synthesized and conjugated to gold nanoparticles (AuNPs) *via* a cathepsin-cleavable linker, GLFGC, to obtain AuNP–Pc158 (Fig. 9c). The AuNP–Pc158 conjugates were inactive and nonfluorescent, while Pc158 released with time upon cathepsin-induced cleavage restored fluorescence and PDT activity. In the *in vivo* study on bearing PC3pip tumours, AuNP–Pc158 presented tumour specificity *via* PSMA targeting, and a sustained release of active Pc158 through cathepsin-activation led to multiple sequential PDT treatments.

Dual stimuli-responsive photosensitizing systems can enhance the tumour specificity, functioning as a molecular "AND" logic gate. Lo *et al.* synthesized a photodynamic molecular beacon (PMB), which could only be activated by the coexistence of matrix metalloproteinase-2 (MMP-2) and cathepsin B (Fig. 9d).[95] In the PMB structure, a distyryl boron dipyrromethene (DSBDP)-based PS and a Black Hole Quencher 3 (BHQ-3) moiety were connected with a cyclized peptide containing sequences PLGVR and GFLG. PMB was largely quenched in normal tissues and even in the presence of one of two enzymes due to the highly efficient Förster resonance energy transfer (FRET) process. In the co-existence of MMP-2 and cathepsin B, PMB was cleaved, and the capability of fluorescence emission and ROS generation was recovered. PMB showed a more significant PDT effect on MMP-2-positive A549 and U-87 MG cells than MMP-2-negative HeLa and HEK-293 cells. The PDT effect of PMB was efficient on the A549 tumor-bearing nude mice model using a diode laser at 680 nm (300 mW cm^{-2}, 10 min), causing no damage to the skin of the mice.

3.1.4 Redox-activated PSs. The basic design principle of redox-activated PSs is based on the different redox potentials between normal and tumour tissues. GSH/glutathione disulfide (GSSG) is the richest redox couple in cells. The GSH concentration in tumour cells is significantly higher than in normal cells,[96] which provokes the construction of GSH-responsive PDT systems. In addition, considering the elevated level of H_2O_2 in the tumours, H_2O_2-activatable PSs have been attracting increasing interest as well.[97,98]

Ng *et al.* reported a thioketal-linked polydopamine (PDA)-based nanosystem (PDA-Dox-Pc-QRH) that could release the immobilised chemotherapeutic and photosensitising drugs (Dox and Pc) upon interactions with the intracellular ROS (Fig. 10a).[99] The disaggregation of the Pc molecules resulted in activation upon excitation with NIR light to generate $^1O_2$. The photodynamic reaction accelerated the degradation of the thioketal-linked structure and the release of larger amounts of therapeutic components. The light-triggered on-demand release of Dox induced additional cytotoxicity through a different pathway and reduced the undesired side effects. PDA-Dox-Pc-QRH showed effective *in vitro* (A549 and A431 cells) and *in vivo* (A431 tumour-bearing nude mice) anticancer activity *via* a synergistic treatment manner including chemotherapy and PDT.

Generally, the therapeutic effect of PDT is weakened by the upregulated antioxidants (GSH in particular) in the tumour cells. Yan *et al.* designed H_2O_2-responsive polymer prodrug nanoparticles (Ce6@P(EG-a-CPBE) NPs) with the GSH-scavenger for chemo-photodynamic synergistic cancer therapy (Fig. 10b).[100] Ce6@P(EG-a-CPBE) NPs were constructed by the co-self-assembly of Ce6 and amphiphilic polymer prodrug P(EG-a-CPBE), which was synthesized from a hydrophilic alternating copolymer P(EG-a-PD) by conjugating hydrophobic anticancer drug chlorambucil (CB) *via* an H_2O_2-cleavable linker 4-(hydroxymethyl)phenylboronic acid (PBA). In the normal tissues, Ce6@P(EG-a-CPBE) NPs were in the "off" state due to the high stability of the PBA linker, while in the tumour tissues, PBA was cleaved rapidly by endogenous H_2O_2 to release CB and Ce6 for a synergistic effect. PBA could be transformed into a GSH-scavenger (quinine methide, QM) under intracellular H_2O_2, thereby preventing the scavenging effect of GSH against

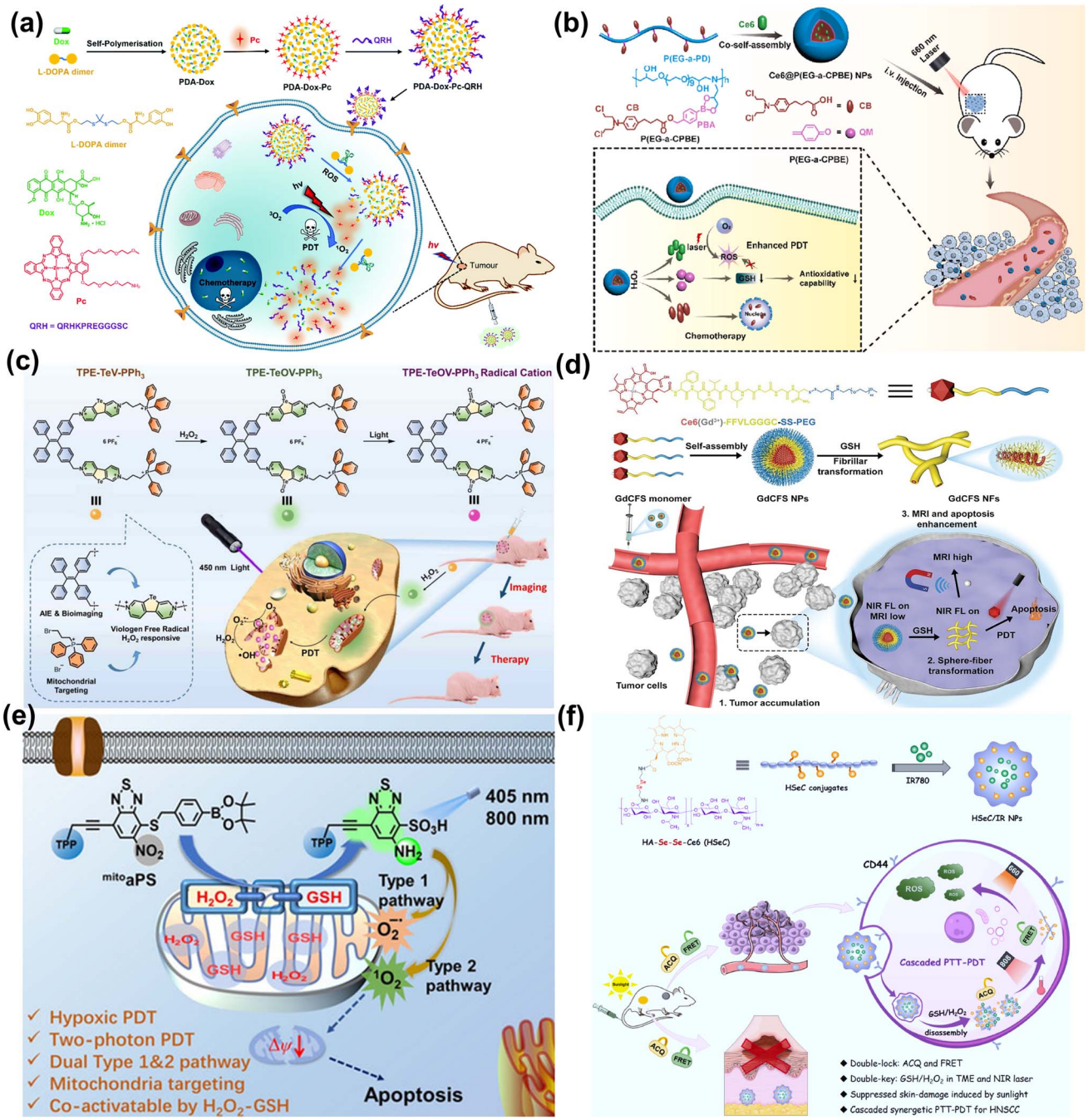

Fig. 10 (a) Formulation of PDA-Dox-Pc-QRH for PDT. Reproduced with permission from ref. 99. Copyright 2021 The Royal Society of Chemistry. (b) Construction of H_2O_2-responsive Ce6@P(EG-a-CPBE) NPs for chemo-PDT synergistic cancer therapy. Reproduced with permission from ref. 100. Copyright 2023 Elsevier B.V. (c) The illustration of TPE–TeV–PPh_3-based H_2O_2-activatable PDT. Reproduced with permission from ref. 101. Copyright 2022 Wiley-VCH. (d) GSH-responsive shape-transformable GdCFS for dual-modal T_1/T_2 MRI-guided enhanced PDT. Reproduced with permission from ref. 102. Copyright 2024 Wiley-VCH. (e) The activatable photosensitizer (^{mito}aPS) for GSH and H_2O_2 mutually responsive PDT. Reproduced with permission from ref. 103. Copyright 2020 Wiley-VCH. (f) Construction of HSeC/IR nanoparticles for cascaded cancer phototherapy. Reproduced with permission from ref. 105. Copyright 2022 Elsevier Ltd.

$^1O_2$ and inducing stronger oxidative stress. The synergistic chemo-photodynamic therapy of Ce6@P(EG-a-CPBE) NPs was efficient in both *in vitro* (MCF-7 cells) and *in vivo* (MCF-7 tumour-bearing mice) studies.

At present, redox-activated PSs with AIE characteristics are drawing increasing interest. In 2022, He *et al.* reported a type-I PS (TPE–TeV–PPh_3) consisting of a tetraphenylethylene group (TPE) as an imaging moiety with AIE properties, triphenylphosphonium (TPP) as a mitochondria-targeting group, and telluroviologen (TeV^{2+}) as a ROS ($O_2^{\bullet-}$, $^{\bullet}OH$) generating moiety. TPE–TeV–PPh_3 was oxidized to luminescent TPE–TeOV–PPh_3 by excess H_2O_2 (Fig. 10c).[101] Exposure of TPE–TeV–PPh_3 to white

light led to killing 7402 cells and MCF-7 cells under normoxia and hypoxia. In the *in vivo* experiments, the tumour growth of 7402-tumour-bearing nude mice was inhibited by 88% after the PDT procedure (450 nm, 200 mW cm^{-2}, 10 min).

In 2024, Huang *et al.* developed a GSH-responsive shape-transformable nanotheranostics Ce6 (Gd^{3+})-FFVLGGGC-SS-PEG (GdCFS) by combining Gd, Ce6 and a peptide (Phe-Phe-Val-Leu-Gly-Gly-Gly-Cys) that was conjugated with polyethylene glycol (PEG) through a disulfide bond, and performed dual-modal T_1/T_2 magnetic resonance imaging (MRI) specifically at the tumour site (Fig. 10d).[102] The spherical GdCFS nanoparticles were responsive to GSH and transformed to nanofibers (NFs), resulting in T_1 positive contrast and T_2 negative contrast enhancement, accompanied by the generation of ROS. Moreover, the depletion of GSH could potentiate PDT efficacy. In the *in vivo* studies, GdCFS presented noticeable proliferation inhibition of tumours in C666-1 tumour-bearing BALB/c nude mice.

In view of the availability of GSH and H_2O_2 in tumours, dual-activatable PDT has advantages in therapeutic controllability. In 2020, our group designed a donor–acceptor type organic PS (^{mito}aPS) which could be co-activated by GSH and H_2O_2 *via* domino reactions on the benzothiadiazole (BTD) ring for mitochondria-targeting PDT (Fig. 10e).[103] The ^{mito}aPS was a precursor of compound NO_2ArSH,[104] and double caging modes were responsible for the molecular activation. First, the fluorescence and photosensitizing properties were caged by the electron-withdrawing nitro group. Second, the thiol group, a precursor of the thiyl radical, was caged by a self-immolative boronic ester that was H_2O_2-specific. The triphenylphosphonium (TPP) ligand-terminated alkyne substituent was attached to the BTD ring to render mitochondria-targeting properties. The ^{mito}aPS was resistant to GSH alone. In the co-existence of GSH and H_2O_2, the uncaged thiol group on the BTD ring by H_2O_2 was oxidized into free radical intermediates that caused intramolecular cyclization and nitro disproportionation. GSH participated in the free radical reaction process through hydrogen atom transfer and accelerated the conversion of ^{mito}aPS into an active PS. One of the advantages using the free radical-relevant thiol chemistry lies in the molecular design free of installation of an active site for GSH, which helps reduce the molecular size of the PDT agent and avoid early uncontrolled activation by GSH. The nitro group of ^{mito}aPS was not reducible by enzyme nitroreductase, guaranteeing reaction selectivity. The mutual activation of ^{mito}aPS by GSH and H_2O_2 in HeLa cells led to "turn on" of both fluorescence and ROS photogeneration, allowing for two-photon excited cellular imaging and hypoxia-tolerant PDT.

In 2022, Qian *et al.* constructed a dual-activatable PDT nanosystem that could be regulated by external NIR laser irradiation and the tumour-specific redox microenvironment

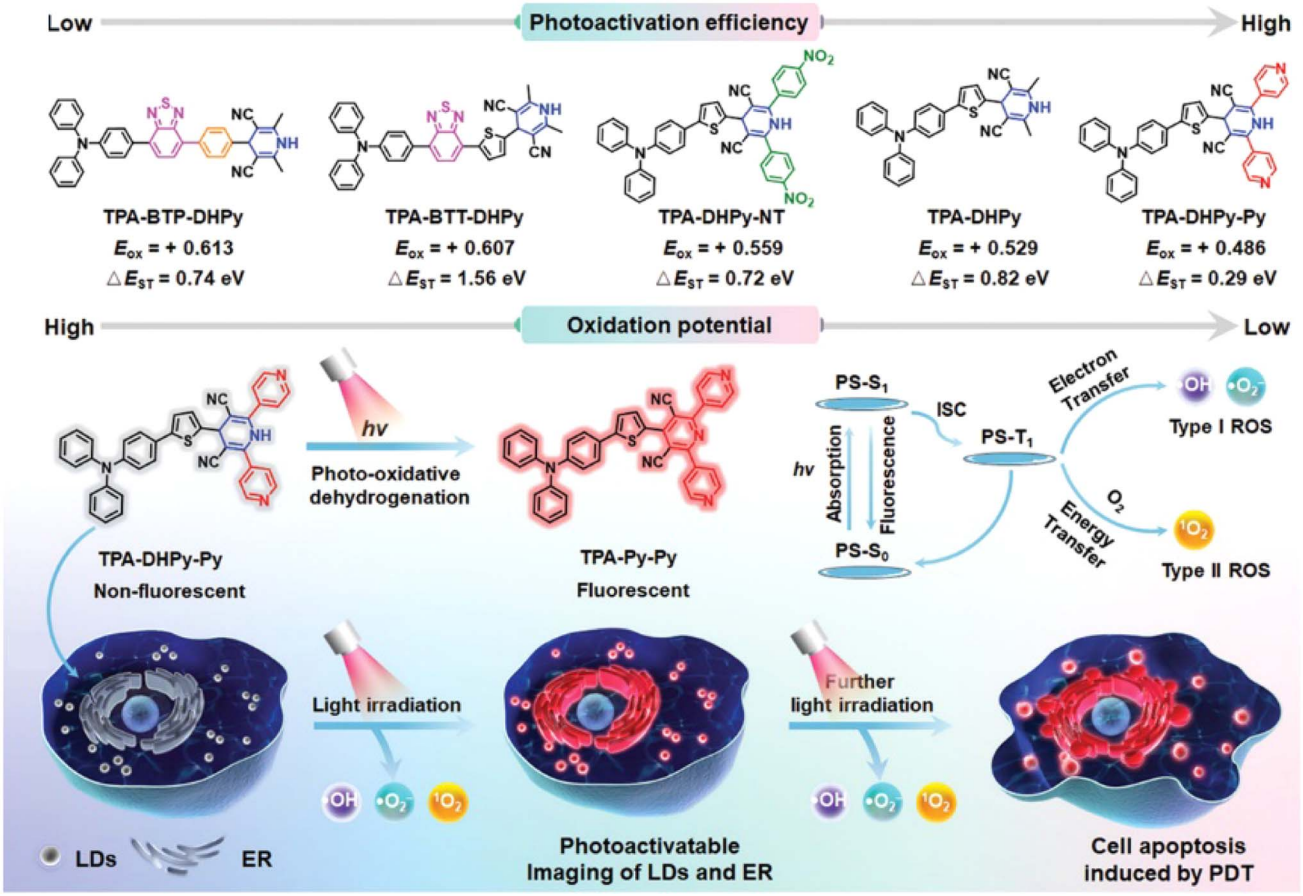

Fig. 11 Photoactivatable theranostic probes for simultaneous imaging of LDs and PDT. Reproduced with permission from ref. 111. Copyright 2022 Wiley-VCH.

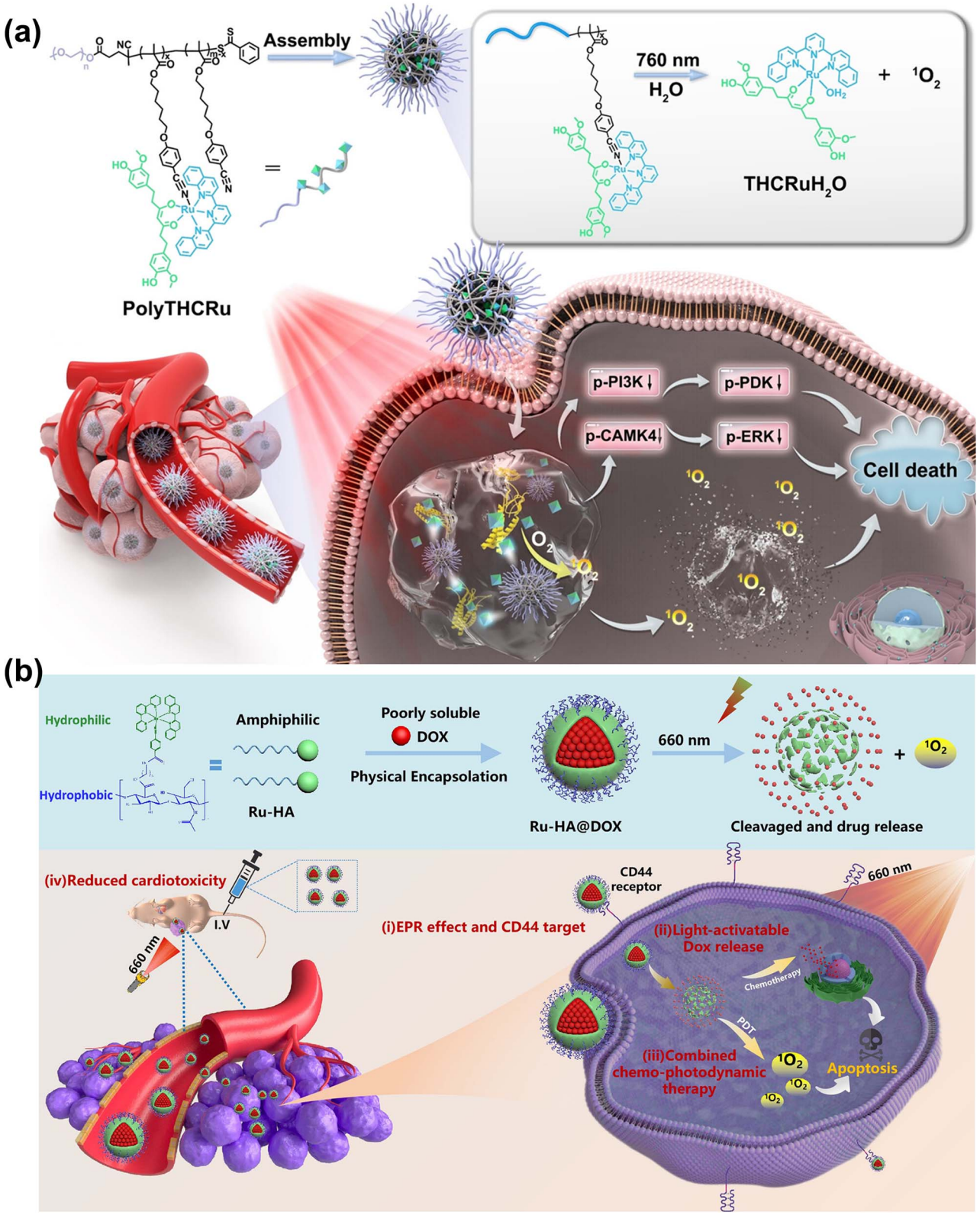

Fig. 12 (a) The photocleavable PolyTHCRu nanoparticles for PDT. Reproduced with permission from ref. 112. Copyright 2023 Wiley-VCH. (b) Formulation of Ru–HA@DOX NPs for chemotherapy–PDT. Reproduced with permission from ref. 113. Copyright 2023 American Chemical Society.

(Fig. 10f).[105] The Ce6 was conjugated to hyaluronic acid (HA) *via* a diselenide linkage to form an amphiphilic polymer (HSeC). The HSeC/IR NPs was assembled from HSeC and IR780 (a PTT agent). During blood circulation, the photoactivity of Ce6 for PDT was "double-locked" by the aggregation-caused quenching (ACQ) effect and FRET from Ce6 to IR780. After selective

accumulation into tumours, HSeC/IR NPs were decomposed due to the dissociation of the diselenide bond in the presence of GSH and H_2O_2. The Ce6 photoactivity was recovered after photothermal degradation of IR780 upon NIR laser irradiation. Consequently, the quenching effect mediated by aggregation and FRET was unlocked by the endogenous redox environment and external NIR light, allowing photoactivation of Ce6 under 660 nm laser irradiation for PDT. HSeC/IR NPs showed low skin 660 nm-photosensitization on the shaved back of healthy mice, while presenting superior tumour suppression *via* synergetic cascaded PTT–PDT in SCC7 tumour-bearing mice.

3.2 Light-activated PSs

Light-responsive PSs have advantages such as spatiotemporal control of drug activation and reduction of side-effects on healthy tissue.[106,107] A variety of light-responsive molecules have been explored for the fabrication of photocages such as derivatives of *o*-nitrobenzyl, phenacyl, BODIPY, cyanine, and Ru complex structures.[32,108–110] In 2021, we established a GSH-light co-responsive PS (DANO) that could be converted to its photoactive form (DAPS), presenting a high performance PDT effect, and a more detailed mechanism is provided in Fig. 3.[45]

In 2022, Tang *et al.* reported a series of triphenylamine (TPA) derivatives based on 1,4-dihydropyridine (1,4-DHPy) as the light-responsive group and optimized photoactivation efficiency by the substituent effect.[111] Amongst these TPA derivatives, TPA–DHPy–Py exhibited the highest photoactivation efficiency (Fig. 11). White light irradiation induced rapid conversion of the non-fluorescent TPA–DHPy–Py into its pyridine counterpart TPA–Py–Py *via* photo-oxidative dehydrogenation, leading to aggregation-induced near-infrared emission. TPA–DHPy–Py presented type I/II combined photodynamic activity, with remarkable ROS production efficiency, and could precisely discriminate cancer cells from co-cultured cells (cancer cells MDA-MB-231 and normal cells NIH-3T3) without the assistance of extra targeting components because of the larger number of lipid droplets (LDs) in the cancer cells. TPA–DHPy–Py was beneficial for *in situ* monitoring of LDs and endoplasmic reticulum alteration under ROS-induced stress. Moreover, the tumour growth of MDA-MB-321-bearing nude mice treated with TPA–DHPy–Py was efficiently inhibited after exposure to white light (30 mW cm^{-2}) for 20 min.

Sun *et al.* constructed a Ru-based photocage (PolyTHCRu) with a NIR light-triggered photocleavage reaction (Fig. 12a).[112] The commercial anticancer drug tetrahydrocurcumin (THC) was coordinated to the Ru(II) center and formed THCRu with significantly enhanced absorption in the NIR region. The THCRu was coordinated to an amphiphilic polymer bearing pendant benzonitrile groups, forming photocleavable Ru–N coordination bonds. The self-assembled polymeric nanoparticle (PolyTHCRu) was sensitive to 760 nm NIR light which induced the dissociation of the Ru(II) complex from the side chains of polymers in the presence of water molecules. In the *in vivo* study, upon 760 nm NIR light irradiation, PolyTHCRu inhibited tumour proliferation on 4T1 tumour-bearing mice *via* combining chemotherapy and PDT. Ding *et al.* developed CD44-targeting and red-light-activatable Ru–HA@DOX NPs through conjugating hydrophilic biodegradable hyaluronic acid (HA) and hydrophobic photoactivatable ruthenium (Ru) complexes (Fig. 12b).[113] Ru–HA@DOX NPs were selectively accumulated at the tumour through an enhanced permeability and retention (EPR) effect and CD44-mediated internalization. Ru–HA@DOX NPs were photolabile at the Ru–N coordination bond under 660 nm laser irradiation, releasing DOX and producing $^1O_2$ for PDT in both *in vitro* (A549 cells) and *in vivo* (A549-tumor-bearing mice) studies.

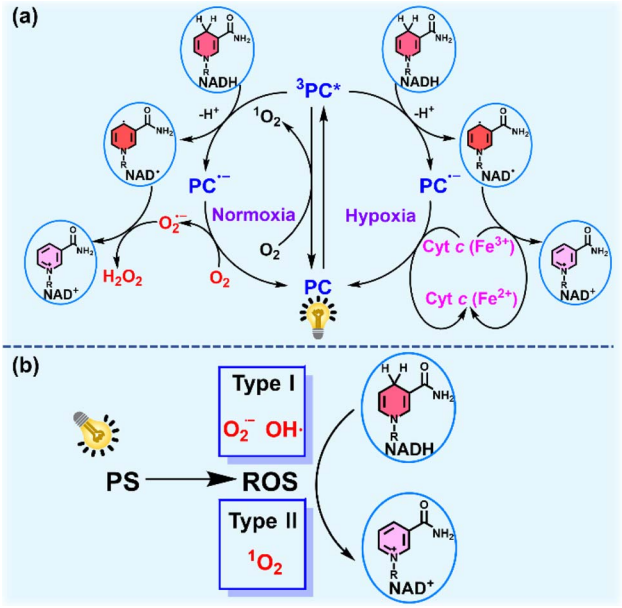

Fig. 13 (a) Plausible mechanism for PC-mediated photocatalytic NADH oxidation under normoxia and hypoxia. (b) Schematic diagram of photocatalytic NADH oxidation *via* ROS produced by PS.

4. Photocatalytic NADH oxidation for PDT

As the electron source of the mitochondrial electron transport chain (mito-ETC), NADH plays an important role in living cells.[114] NADH participates in the maintenance of the intracellular redox balance and functions as a coenzyme in over 400 oxidoreductases.[71,115] Photoredox catalysis for NADH oxidation to perturb the NADH/NAD^+ balance and the electron flow in intracellular mito-ETC is emerging as a novel strategy to induce metabolic dysfunction and cell death.

Photocatalysts (PCs) including metal complexes, organic compounds and nano-catalysts catalyze NADH oxidation mainly through two pathways. One is based on a photocatalytic cycle (Fig. 13a).[116] The photoexcited PC extracts an electron from NADH, forming the anionic radical $PC^{\bullet-}$ and $NAD^\bullet$ radical. In the presence of oxygen, PC is regenerated with concomitant production of $O_2^{\bullet-}$ after electron transfer from $PC^{\bullet-}$ to oxygen. Then $O_2^{\bullet-}$ extracts an electron from $NAD^\bullet$ and consumes two protons from the medium to generate H_2O_2, accompanied by the conversion of $NAD^\bullet$ into NAD^+. Under hypoxia, hemoprotein

cytochrome *c* (Cyt *c* (Fe^{3+})) acts as a terminal electron acceptor to enhance the PDT effect *via* an O_2-independent pathway. Another pathway for photocatalytic NADH oxidation is available through photogeneration of ROS which oxidize NADH to NAD^+ (Fig. 13b).[117] In this section, recent progress on photocatalytic NADH oxidation for PDT *via* the above two pathways will be discussed.

4.1 Metal complexes

Transition metal complexes have attractive photochemical and photophysical properties (*e.g.*, excellent photostability, long excited-state lifetime and suitable excited-state reduction potential),[6,23] available by coordinating ligands to metal ions in a combinatorial manner.[6] The use of transition metal complexes for photocatalytic NADH oxidation is of increasing interest in PDT.[118] We will focus on the recent approaches harnessing transition metal complexes such as Ir(III), Ru(II) and Os complexes for PDT *via* NADH oxidation.

4.1.1 Ir(III) complexes. In 2019, Sadler *et al.* reported pioneering work on interfering the electron flow in intracellular mito-ETC *via* photoredox catalytic NADH oxidation and Cyt *c* (Fe^{3+}) reduction to enhance PDT in hypoxic tumours, using a stable Ir(III) photocatalyst (complex 1) with a relatively positive excited-state reduction potential (Fig. 14a).[116] Complex 1 could photo-oxidize NADH to $NAD^{\bullet}$ with turnover frequency (TOF) more than two orders of magnitude higher than that of organometallic half-sandwich catalysts, and was responsible for disrupting electron transfer pathways in mitochondria to promote redox imbalance due to its accumulation in mitochondria. Under normoxia, dramatic depletion of NADH and ATP occurred after photoexcitation of complex 1. Of note, complex 1 also exhibited high photocytotoxicity towards A549 lung cancer multicellular spheroids (MCSs) under hypoxia by disrupting the mitochondrial membrane potential (MMP) and inducing immunogenic apoptotic cell death.

To date, a variety of Ir(III) complexes have been developed to obtain longer wavelengths and improve biocompatibility. Huang *et al.* reported a water-soluble coumarin-functionalized Ir(III) photocatalyst (Ir3) that absorbed visible light (Fig. 14b).[119] Compared with Ir1 and Ir2, Ir3 presented high TOF (308.0 h^{-1}) on NADH oxidation under normoxia. Ir3 induced remarkable photo-triggered cytotoxicity against various cancer cell lines (1–15 μM), while maintaining low toxicity (>100 μM) on normal cells in the dark. Huang's group further designed three glucose-appended cyclometalated Ir(III) complexes (Ir4–Ir6) containing the *N*,*N*-glucose ligand and various *N*,*C*-ligands to optimize their photochemical properties and non-glycosylated complex Ir7 (Fig. 14c).[120] Ir6 presented the strongest aqueous solubility and the highest photocatalytic NADH oxidation efficiency, exhibiting necro-apoptotic photocytotoxicity on HeLa cells at sub-micromolar concentrations upon light irradiation. Espino *et al.* prepared four Ir(III) biscyclometallated complexes with N^N′ ancillary ligands containing an amide-substituted benzimidazole fragment and pyridine

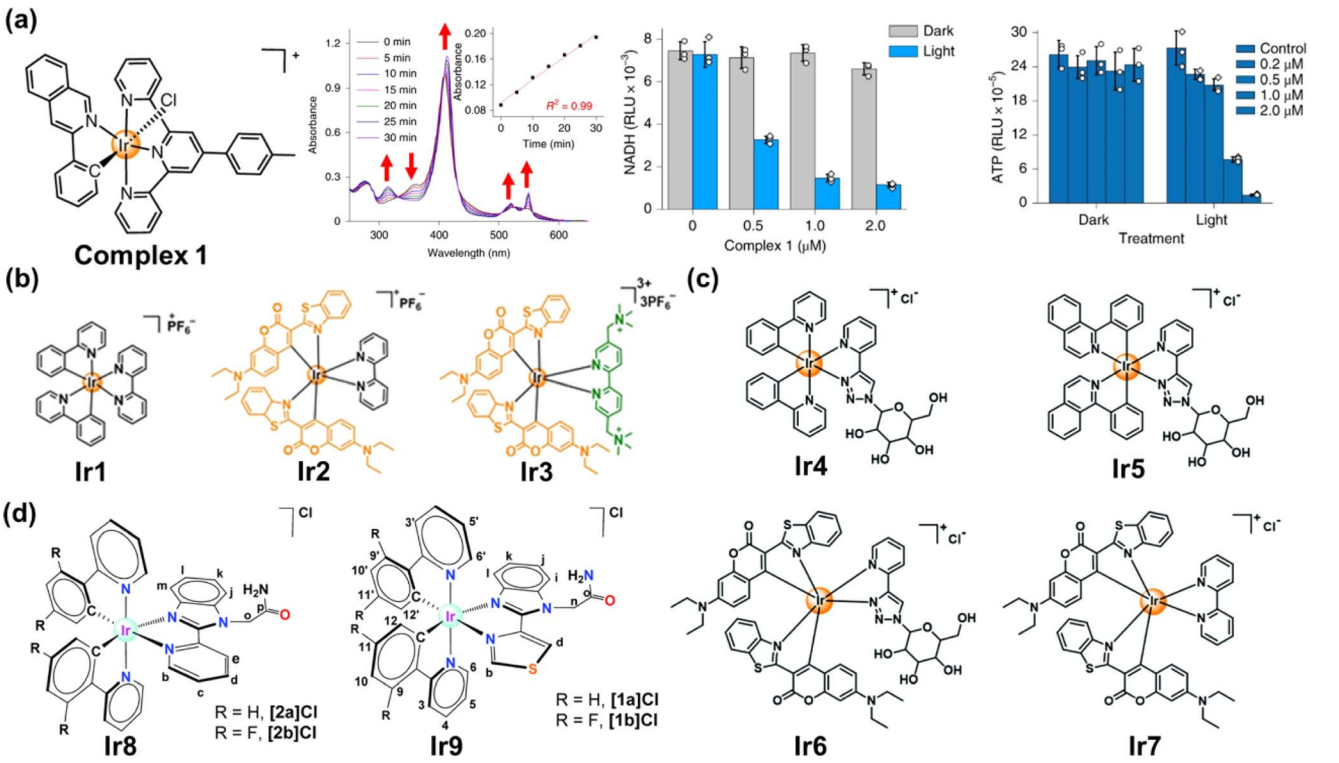

Fig. 14 (a) The complex 1 used for photocatalytic NADH oxidation. Reproduced with permission from ref. 116. Copyright 2019 Springer Nature. (b–d) The complexes Ir1–Ir9 used for photocatalytic NADH oxidation. Reproduced with permission from ref. 119. Copyright 2021 Wiley-VCH. Reproduced with permission from ref. 120 and 121. Copyright 2022 The Royal Society of Chemistry.

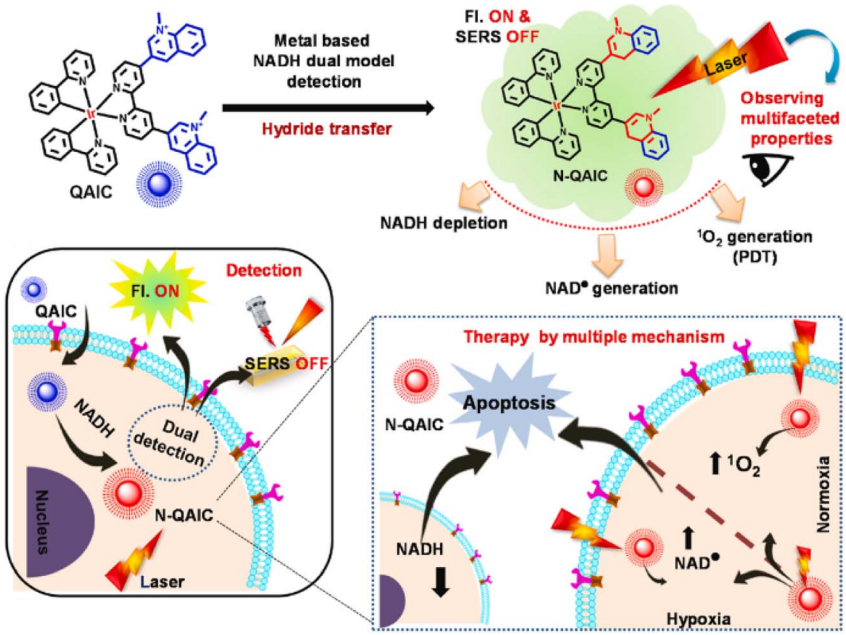

Fig. 15 The mechanism of NADH detection with QAIC and laser triggered therapeutic mechanism of N-QAIC. Reproduced with permission from ref. 124. Copyright 2022 Elsevier B.V.

(Ir8) or thiazolyl (Ir9) rings (Fig. 14d).[121] [1a]Cl and [2a]Cl were accumulated primarily in mitochondria, disrupting electron transport *via* NADH photocatalytic oxidation and presumably inducing mtDNA damage.

Altered cellular metabolism is a hallmark of cancer, where NADH plays an important role in the excess energy required for various anaplerotic reactions.[122,123] Maiti *et al.* reported a quinoline appended Ir(III) complex (QAIC) as a molecular probe to detect endogenous NADH in cancer cells *via* the "turn-on" luminescence and "turn-off" SERS phenomenon (Fig. 15).[124] QAIC could recognize the dynamic fluctuations of NADH and trigger PDT through NADH depletion. The activated N-QAIC in the cellular milieu presented excellent phototoxicity on HepG2 cells by the generation of $^1O_2$ under normoxia and toxic NAD$^\bullet$ under hypoxia.

4.1.2 Ru(II) complexes. Photoactive Ru(II)-based complexes have been widely utilized for the light-driven anticancer effect through PDT, photochemotherapy (PCT) and photoredox catalysis.[125,126] The Ru(II) polypyridyl complex, TLD-1433, is currently in clinical trials for PDT.[127]

Zhou *et al.* constructed a PCT system *via* the use of a Ru(II) complex and Fe(tpy)Cl_3 (tpy = 2,2′:6′,2′-terpyridine).[128] The Ru(II) complex photocatalyzed NADH oxidation accompanied by the generation of H_2O_2 *in situ* with a high yield of 73.2%. At a neutral pH, the decomposition of H_2O_2 was mediated by Fe(tpy)Cl_3 and afforded highly cytotoxic $^\bullet$OH. To extend the excitation light from blue light into the NIR region, the same group loaded the Ru(II) complex (Ru_1) and Fe^{2+} simultaneously onto the mesoporous silica-encapsulated rare earth-doped upconversion nanoparticles (Fig. 16a).[129] Moreover, Zhou's group designed a chloromethyl-modified Ru(II) complex as a mitochondria targeting PS to overcome the limitation of hypoxia in PDT,[130] which could be photoexcited to generate a carbon radical in the presence of NADH, accompanied by the oxidation of NADH, thereby giving rise to DNA damage and cancer cell inactivation under hypoxia (3% O_2).

In 2023, Sadler *et al.* reported a hypoxia-activated mitochondria-accumulated Ru(II) polypyridyl prodrug, RuAzNM, that was functionalized with an azo group and a nitrogen mustard moiety for multimodal theranostic studies (Fig. 16b).[131] In hypoxic tumour microenvironments, the azo group was reduced selectively by reductase and cleaved to generate two primary amine products including the aniline mustard and polypyridyl $RuNH_2$ complex. The aniline mustard triggered oxidative stress and mtDNA crosslinking. Meanwhile, the polypyridyl $RuNH_2$ complex catalyzed NADH oxidation based on its favorable excited-state photoredox potential and superior binding affinity toward NADH. This multimodal therapeutic manner presented an efficient inhibition effect on the HepG2 MCS model.

4.1.3 Os complexes. Osmium complexes emit intense infrared phosphorescence and have strong light stability, which provides an anti-biological-background-interference ability.[132,133] The structural plasticity allows applications of osmium complexes in bioimaging and PDT.[132–134] Zhang *et al.* reported three mitochondria-targeting NIR terpyridine Os(II) complexes.[135] The increased conjugate plane of the terpyridine ligand caused enhanced NIR phosphorescence emission and prolonged phosphorescence lifetime (Fig. 17a). The complexes produced $^1O_2$ efficiently upon both 465 nm and 633 nm light irradiation and were used for the strong PDT effect against HepG2 cells by photo-oxidation of NADH into NAD^+. In 2022, Zhang *et al.* designed another osmium–peroxo complex (Os2), which was inactive in the dark.[117] Light irradiation of Os2 led to

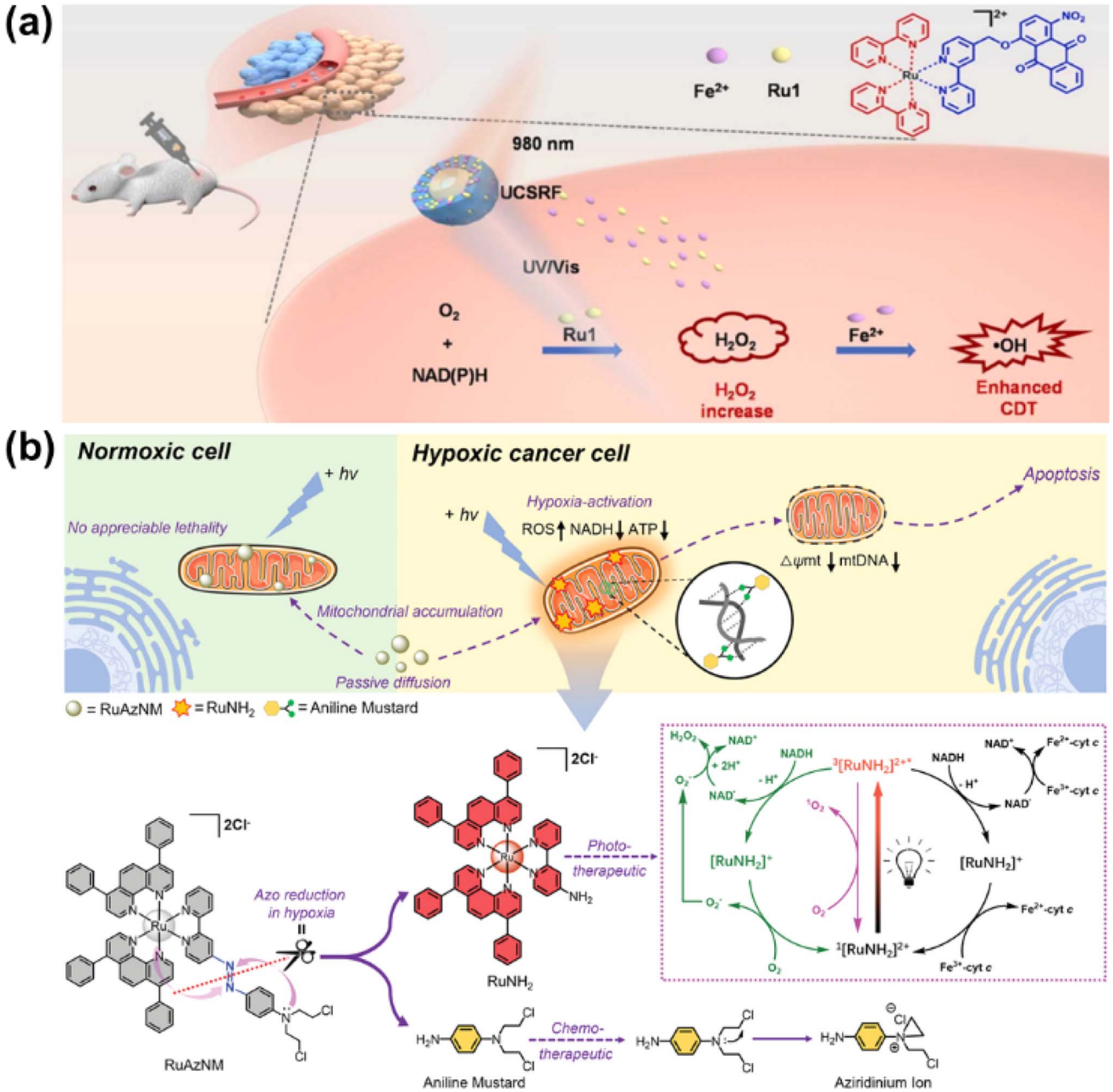

Fig. 16 (a) The UCSRF nanoparticle for NIR light-driven photocatalytic NADH oxidation. Reproduced with permission from ref. 129. Copyright 2023 Elsevier Ltd. (b) The prodrug RuAzNM used for chemotherapy and PDT. Reproduced with permission from ref. 131. Copyright 2023 Wiley-VCH.

the release of $O_2^{\bullet-}$ even in severely hypoxic conditions (1% O_2) and generated a cytotoxic osmium complex (Os1) (Fig. 17b). Disproportion of $O_2^{\bullet-}$ by superoxide dismutase (SOD) afforded H_2O_2 and O_2. The $^{\bullet}OH$ was derived from H_2O_2 at Fe^{2+} exposure. Photo-oxidation of NADH was mediated by Os2 *via* two pathways including NADH/photoexcited Os1 interaction and oxidation by $O_2^{\bullet-}$. The downregulation of NADH indirectly affected the reduction of GSSG to GSH by glutathione reductase, leading to the accumulation of lipid peroxides and ultimately the synergistic induction of ferroptosis. *In vivo* studies confirmed that the Os2 could inhibit the growth of solid hypoxic tumours in HeLa tumour-bearing BALB/c mice after light irradiation (465 nm, 13 mW cm^{-2}, 60 min).

4.2 Organic metal-free photocatalysts

For metal complexes, unpredicted metal toxicity, inferior biostability, and limited tissue penetration (UV, blue or green light excitation) arouse concerns in the biomedical field.[136,137] Organic photocatalysts alleviate potential metal-associated concerns. At present, the application of organic molecules has emerged as photocatalytic anticancer agents.

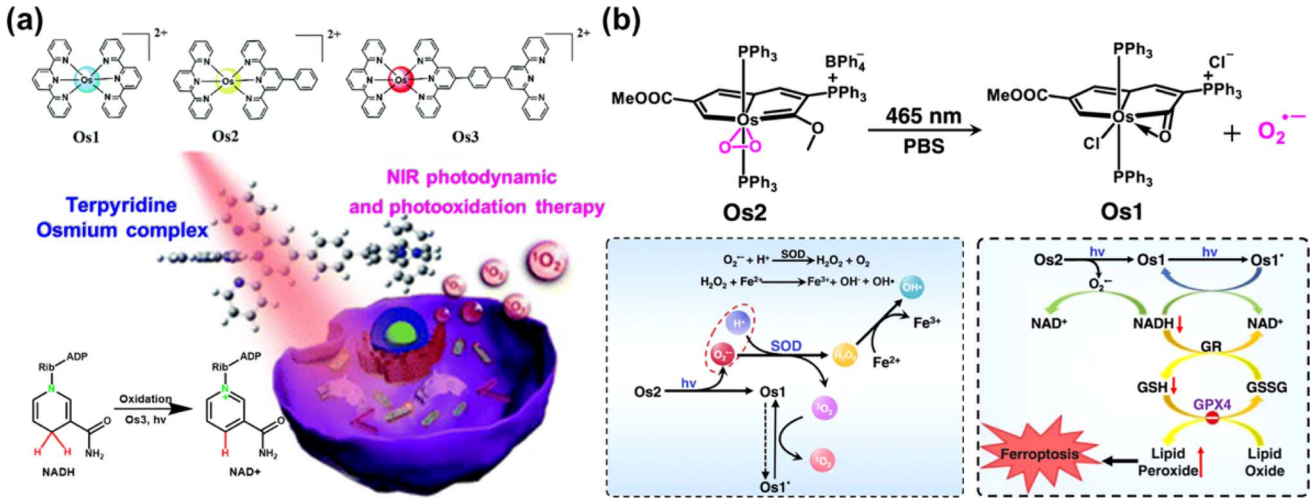

Fig. 17 (a) The Os(II)-terpyridine complexes used for PDT and photooxidation therapy. Reproduced with permission from ref. 135. Copyright 2020 The Royal Society of Chemistry. (b) The photocatalytic NADH oxidation by light-activating Os2. Reproduced with permission from ref. 117. Copyright 2022 Springer Nature.

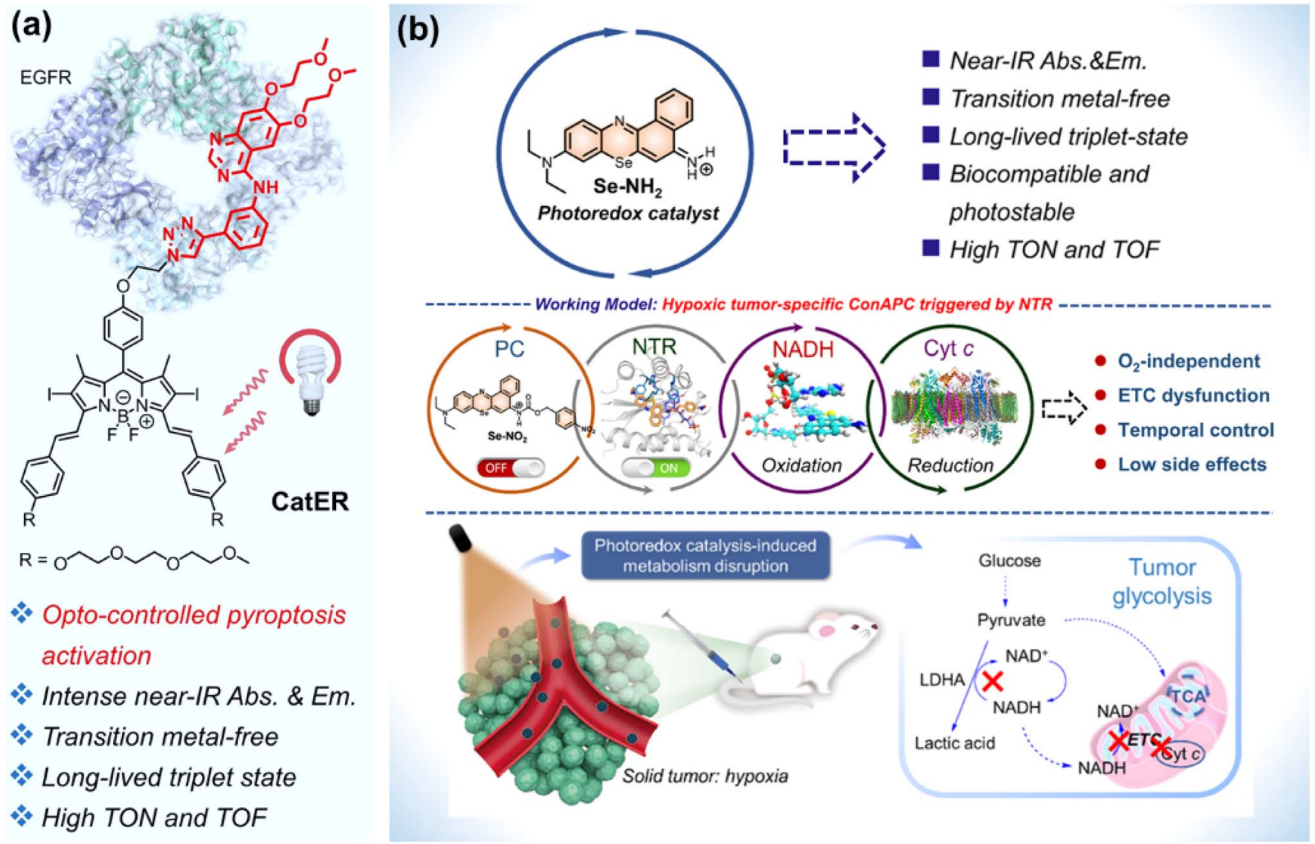

Fig. 18 (a) CatER-based photocatalytic NADH oxidation. Reproduced with permission from ref. 139. Copyright 2022 National Academy of Science. (b) Se–NH_2 based photoredox catalysis for phototherapy against a hypoxic solid tumour. Reproduced with permission from ref. 140. Copyright 2022 American Chemical Society.

Huang *et al.* designed compound bpyPCN with favourable aqueous solubility. The significant PDT performance was ascribed to its excellent ability for $^1O_2$ generation and photocatalytic NADH oxidation.[138] To render the absorption of photocatalysts for photoredox catalysis in the NIR spectral range, Kim *et al.* conjugated a BODIPY moiety to erlotinib (ER, an FDA-approved tyrosine kinase inhibitor) to obtain a photocatalyst (CatER) (Fig. 18a).[139] Under normoxia, photoactivation

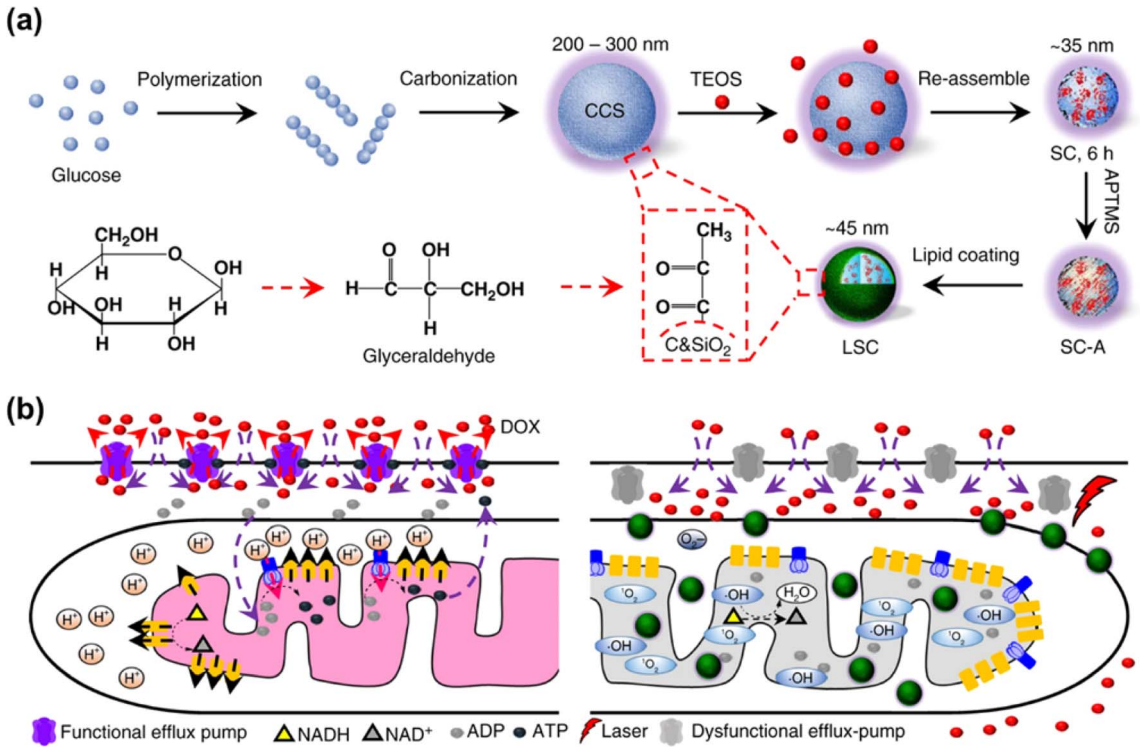

Fig. 19 (a) Formulation of LSC NPs. (b) Application of LSC NPs for overcoming the cancer drug resistance. Reproduced with permission from ref. 147. Copyright 2018 Springer Nature.

of CatER gave rise to $^1O_2$ production and NADH oxidation with high TOF (49.3 min^{-1}). *In vitro* studies revealed that CatER exhibited light dose-dependent depletion of NADH and a high level of antiproliferation activity toward A549 cells with NIR irradiation. Additionally, tumour growth was significantly suppressed in BALB/c mice bearing 4T1 tumours.

Considering the off-target risk and safety concerns of photocatalysts in living systems, Peng *et al.* explored a conditionally activatable photoredox catalysis (ConAPC) system and designed ConAPC architecture (Se–NO_2) in which the inherent photocatalytic properties were temporarily caged (Fig. 18b).[140] Se–NO_2 was converted to Se–NH_2 by the overexpressed nitroreductase (NTR) in tumours. Se–NH_2 was activated by NIR light and catalyzed NADH oxidation with high TOF (18.8 min^{-1}), which triggered the reductive transformation of Cyt *c* (Fe^{3+}). The hypoxic tumour-specific ConAPC system proceeded independently on O_2, and the anti-cancer activity toward hypoxic tumours was achieved through perturbing the mitochondrial respiration ETC and cellular metabolism. In the *in vivo* PDT experiments on HeLa-tumour-bearing female BALB/c mice, the tumour growth inhibition up to 91% was obtained. This work offers a possibility by leveraging artificial photocatalytic reactions toward the development of facile and intelligent photocatalytic theranostics.

4.3 Nano-catalysts

The EPR effect has been recognized as the central paradigm in tumour-targeted delivery in the past few decades.[141] Especially, nano-based drug delivery systems are more beneficial to enhance the EPR effect of the tumour vasculature for *in vivo* tumour targeting to reduce the systemic toxicity. Recent studies on photocatalytic NADH oxidation using nano-catalysts demonstrate great potential in photoredox catalysis for PDT.[142–144]

Multidrug resistance is a major challenge in chemotherapy and its phenotype is associated with the overexpression of ATP-driven transmembrane efflux pumps in cancer cells.[145,146] Therefore, cancer drug resistance can be overcome by inhibiting the production of ATP in cancer cells, which is achievable through oxidizing NADH into NAD^+. In 2018, He *et al.* reported a lipid membrane-coated silica–carbon (LSC) hybrid nanoparticle that targeted mitochondria through pyruvate (Fig. 19a).[147] Doxorubicin (DOX) was encapsulated into the LSC NPs to form LSC-D NPs. The size of the LSC-D NPs (~45 nm) was suitable for the requirement of the EPR effect for *in vivo* tumour targeting. Upon NIR laser (800 nm) irradiation of the LSC-D NPs, ROS was generated and the oxidation of NADH into NAD^+ caused a reduction in the amount of ATP available for the efflux pump. Consequently, multidrug-resistant cancer cells lost their multidrug resistance capability for at least 5 days due to the compromised drug efflux pumps, which created a therapeutic window for chemotherapy (Fig. 19b). The *in vivo* data showed that the LSC-D NPs in combination with NIR laser treatment effectively inhibited the growth of multidrug-resistant tumours (nude mice with NCI/RES-ADR xenograft) without evident systemic toxicity. This study

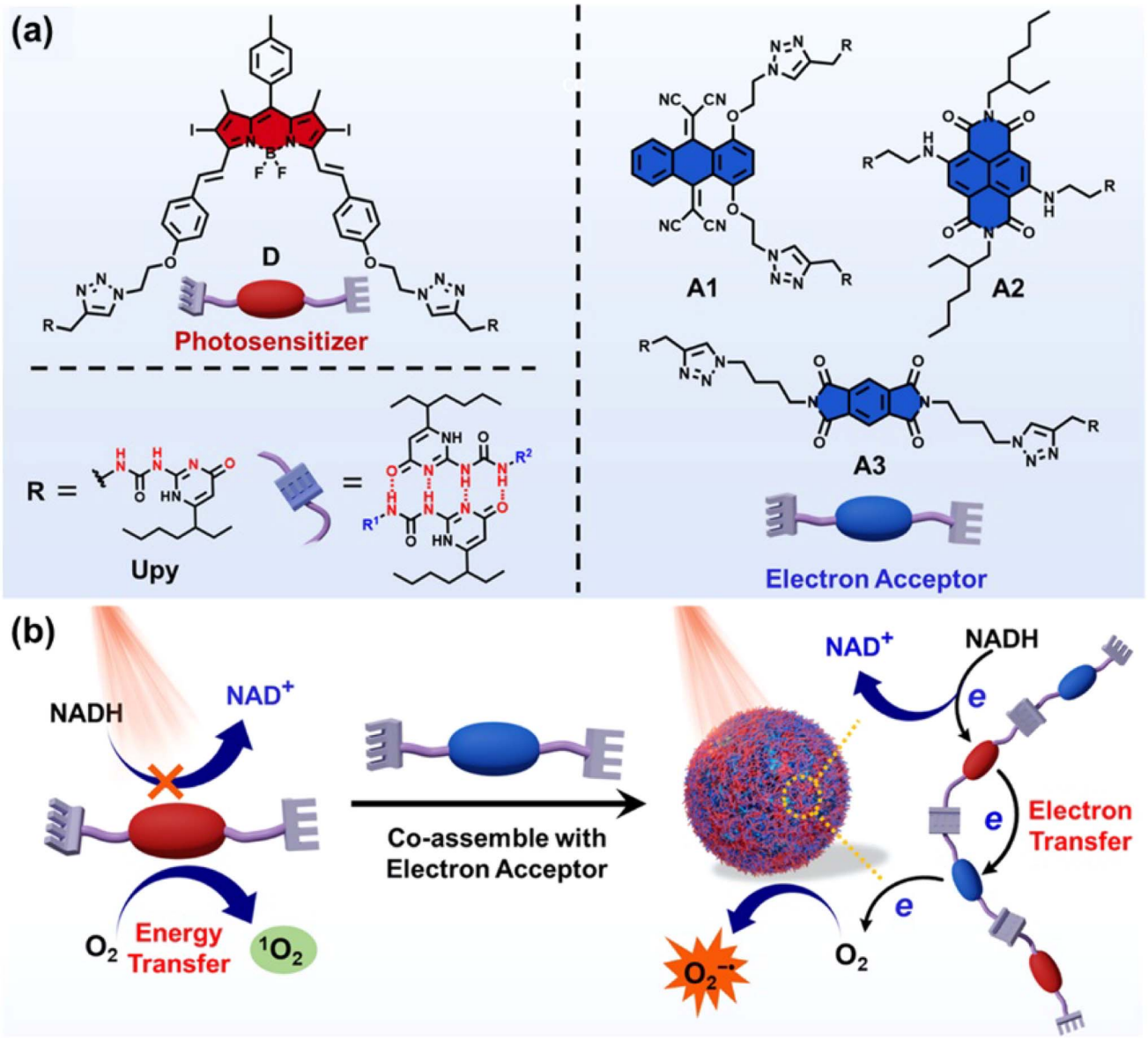

Fig. 20 (a) Chemical structures of the photosensitizer (D) and electron acceptors (A1, A2, and A3). (b) Supramolecular photodynamic system for photo-induced oxidation of NADH and generation of $O_2^{\bullet -}$. Reproduced with permission from ref. 148. Copyright 2022 Springer Nature.

provides a promising nanotechnology-based strategy for fighting cancer multidrug resistance *via* photocatalytic NADH oxidation.

In 2022, Yang *et al.* reported a new strategy to boost the type-I PDT reaction by introducing electron acceptors to the existing type-II PS through the supramolecular assembly.[148] Three different types of electron acceptors were co-assembled with a type-II PS to form quadruple hydrogen-bonded supramolecular photodynamic agents (DA1, DA2 and DA3) (Fig. 20a). Upon light irradiation of 660 nm, electron transfer took place from the PS to the electron acceptor and then to O_2, which led to an efficient production of $O_2^{\bullet -}$. In addition, this process was accompanied by the generation of a strong oxidizing cationic radical of the PS ($PS^{+\bullet}$) that was able to oxidize NADH into NAD^+ (Fig. 20b). The supramolecular systems showed excellent activities of photocatalytic NADH oxidation (24.8 min^{-1} for DA1, 53.7 min^{-1} for DA2, 24.3 min^{-1} for DA3). As a result, the supramolecular PS exhibited superior PDT performance in treating tumours at *in vitro* and *in vivo* (a subcutaneous tumour model of HeLa in the BALB/c mice) levels. This work will broaden the insight into type-I PDT and inspire researchers to develop effective nano-catalysts for tumour therapy.

5. Conclusions and future prospects

This review has systematically discussed most recent strategies for PDT based on new mechanisms, including (1) developing novel radicals to reduce the dependence on O_2; (2) designing activatable PSs on tumour cells to minimize damage to normal cells; (3) photocatalytic NADH oxidation to perturb the electron flow in intracellular mito-ETC.

At present, fortunately, some strategies based on new mechanisms have drawn interest in clinical trials. TLD-1433 is the first Ru-based PS and has completed a phase I clinical trial for the treatment of bladder cancer. The phase II clinical study of TLD-1433 commenced in 2019 in the USA and Canada with a plan to treat 100–125 patients who developed nonmuscle invasive bladder cancer (NMIBC) and are intolerant or unresponsive to bacillus Calmette Guérin (BCG) therapy.[149,150] Phototherapy and immunotherapy in combination, namely photoimmunotherapy (PIT), is emerging as a promising therapeutic strategy to both primary and metastatic tumours. PIT utilizes the PDT effect to induce systemic immune responses against tumours,[151] maximizing the merits of both therapy modalities, leading to long-term immunity against cancer and increasing the selectivity of cancer therapy. Cetuximab sarotalocan (RM-1929), the first PIT drug in clinical trial, is an antibody–drug conjugate (ADC) carrying cetuximab and organic dye IRdye700DX, which can be activated by NIR irradiation at 690 nm to induce PDT and stimulate the anti-cancer immune response. Currently, cetuximab sarotalocan is being investigated under a world-wide phase III clinical trial and has been conditionally approved in Japan in 2020 for the treatment of unresectable locally advanced or unresectable locoregionally recurrent head and neck carcinoma (HNC).[152] Based on the clinical trials of RM-1929 in PIT, in 2023, Mitsunaga *et al.* discussed abundant cases on how to set up and perform PIT applications *in vitro* and *in vivo* from a lot of aspects such as source of antibody, choice of dye and target, and methods used to characterize the labeled antibody, which is useful for targeted elimination of microbes and cells regardless of the target species or drug resistance status of the target.[153] Other clinical trials based on innovative PDT are also under process. For example, Roswell Park Cancer Institute Corp put forward a phase I study utilizing PDT to amplify the response to immunotherapy in patients with non-small cell lung cancer (NSCLC) with pleural disease or malignant pleural mesothelioma (NCT04836429). The Mayo Clinic Foundation has proceeded with a phase II study of EUS-guided Verteporfin PDT in solid pancreatic tumours (NCT03033225).

However, most PDT strategies are in the basic research or preclinical phase, and there is a long way to go for clinical applications. One of the major challenges is the development of deep-tissue PDT, which needs to develop PSs with strong absorption in the deep red or NIR regions. Although two-photon excitation has been used to enhance the penetration depth of PDT and improve spatial selectivity, their clinical application is hindered due to the requirement of expensive devices and limitation in the excited domain. Thus, developing chemiluminescence/bioluminescence-based PSs for PDT will be a promising direction. Another important concern is how to improve the tumour-selectivity in PDT theranostics to maximize the therapeutic effect while minimizing damage to normal tissues, which will inspire increasing efforts in harnessing tumour biomarkers (hypoxia, GSH, ROS, NADH, enzyme, pH, *etc.*) to selectively activate PSs or convert precursors into PSs in tumours. Exogenous 5-ALA is a good case for imaging-guided PDT with good tumour selectivity, as it can be converted into protoporphyrin IX (PpIX), a fluorogenic PS, *via* a biosynthetic pathway in the tumour cells. In 2022, we reported an example of in-cell synthesis of a trimethine cyanine-type PDT agent *via* a pseudo-trimerization mechanism using an exogenous iodo-substituted indole derivative as a precursor and intrinsic ROS as the inducer, which provides an opportunity for imaging-guided PDT by taking advantage of the redox environment of tumours.[154]

Importantly, regarding the efficacy of PDT, the barrier of heterogeneous tumour hypoxia, which affects most clinically used PDT agents, highlights the need to develop new PSs that are active in type I or non-classic photosensitizing mechanisms with minimal oxygen dependence. The exploration of active free radicals for PDT beyond ROS and RNS provides an opportunity to evade the barrier of heterogeneous tumour hypoxia. So far, the intermediates produced in the regular PDT process cover a large scope of reactive oxidative species to treat cancers by photo-oxidative damage. Opposite to the photo-oxidative strategy, reactive reductive species (RRS)-involving PDT is free of O_2 dependence and has started to attract attention, which leaves plenty of research space in understanding the biological functions of RRS, designing efficient RRS generators and aiming at hypoxic cancers with satisfactory selectivity and efficacy.

Data availability

No primary research results, software or code have been included and no new data were generated or analysed as part of this review.

Author contributions

X. W. and F. F. conceived the idea. X. W., J. P. and C. M. contributed to the writing of the original draft of the manuscript. F. F. reviewed and revised the manuscript.

Conflicts of interest

There are no conflicts to declare.

Acknowledgements

We thank the National Natural Science Foundation of China (22277054, 22077065) for financial support.

Notes and references

1 H. Sung, J. Ferlay, R. L. Siegel, M. Laversanne, I. Soerjomataram, A. Jemal and F. Bray, *Ca-Cancer J. Clin.*, 2021, **71**, 209–249.
2 H. J. Burstein, *J. Clin. Oncol.*, 2000, **18**, 693.
3 E. Rullier, P. Rouanet, J.-J. Tuech, A. Valverde, B. Lelong, M. Rivoire, J.-L. Faucheron, M. Jafari, G. Portier, B. Meunier, I. Sileznieff, M. Prudhomme, F. Marchal, M. Pocard, D. Pezet, A. Rullier, V. Vendrely, Q. Denost, J. Asselineau and A. Doussau, *Lancet*, 2017, **390**, 469–479.

4 K. Wang and J. E. Tepper, *Ca-Cancer J. Clin.*, 2021, **71**, 437–454.
5 J. Tian, B. Huang, M. H. Nawaz and W. Zhang, *Coord. Chem. Rev.*, 2020, **420**, 213410.
6 X. Zhao, J. Liu, J. Fan, H. Chao and X. Peng, *Chem. Soc. Rev.*, 2021, **50**, 4185–4219.
7 D. E. J. G. J. Dolmans, D. Fukumura and R. K. Jain, *Nat. Rev. Cancer*, 2003, **3**, 380–387.
8 S. Kim, T. Tachikawa, M. Fujitsuka and T. Majima, *J. Am. Chem. Soc.*, 2014, **136**, 11707–11715.
9 X. Li, Y. Zhao, T. Zhang and D. Xing, *Adv. Healthcare Mater.*, 2021, **10**, 2001240.
10 S. Fulda, L. Galluzzi and G. Kroemer, *Nat. Rev. Drug Discovery*, 2010, **9**, 447–464.
11 G. Yang, L. Xu, J. Xu, R. Zhang, G. Song, Y. Chao, L. Feng, F. Han, Z. Dong, B. Li and Z. Liu, *Nano Lett.*, 2018, **18**, 2475–2484.
12 X. Guo, N. Yang, W. Ji, H. Zhang, X. Dong, Z. Zhou, L. Li, H.-M. Shen, S. Q. Yao and W. Huang, *Adv. Mater.*, 2021, **33**, 2007778.
13 C. S. Foote, *Photochem. Photobiol.*, 1991, **54**, 659.
14 M. S. Baptista, J. Cadet, P. Di Mascio, A. A. Ghogare, A. Greer, M. R. Hamblin, C. Lorente, S. C. Nunez, M. S. Ribeiro, A. H. Thomas, M. Vignoni and T. M. Yoshimura, *Photochem. Photobiol.*, 2017, **93**, 912–919.
15 Y.-Y. Wang, Y.-C. Liu, H. Sun and D.-S. Guo, *Coord. Chem. Rev.*, 2019, **395**, 46–62.
16 W. Fan, P. Huang and X. Chen, *Chem. Soc. Rev.*, 2016, **45**, 6488–6519.
17 M. Dichiara, O. Prezzavento, A. Marrazzo, V. Pittalà, L. Salerno, A. Rescifina and E. Amata, *Eur. J. Med. Chem.*, 2017, **142**, 459–485.
18 I. J. Macdonald and T. J. Dougherty, *J. Porphyrins Phthalocyanines*, 2001, **5**, 105–129.
19 M. C. DeRosa and R. J. Crutchley, *Coord. Chem. Rev.*, 2002, **233**, 351–371.
20 S. Kwiatkowski, B. Knap, D. Przystupski, J. Saczko, E. Kędzierska, K. Knap-Czop, J. Kotlińska, O. Michel, K. Kotowski and J. Kulbacka, *Biomed. Pharmacother.*, 2018, **106**, 1098–1107.
21 P. Agostinis, K. Berg, K. A. Cengel, T. H. Foster, A. W. Girotti, S. O. Gollnick, S. M. Hahn, M. R. Hamblin, A. Juzeniene, D. Kessel, M. Korbelik, J. Moan, P. Mroz, D. Nowis, J. Piette, B. C. Wilson and J. Golab, *Ca-Cancer J. Clin.*, 2011, **61**, 250–281.
22 T. Hu, Z. Wang, W. Shen, R. Liang, D. Yan and M. Wei, *Theranostics*, 2021, **11**, 3278–3300.
23 Y. Wu, S. Li, Y. Chen, W. He and Z. Guo, *Chem. Sci.*, 2022, **13**, 5085–5106.
24 Z. Zhou, J. Song, L. Nie and X. Chen, *Chem. Soc. Rev.*, 2016, **45**, 6597–6626.
25 Z. Yu, P. Zhou, W. Pan, N. Li and B. Tang, *Nat. Commun.*, 2018, **9**, 5044.
26 H. Li, X. Fan and J. Houghton, *J. Cell. Biochem.*, 2007, **101**, 805–815.
27 D. F. Quail and J. A. Joyce, *Nat. Med.*, 2013, **19**, 1423–1437.
28 W.-L. Liu, T. Liu, M.-Z. Zou, W.-Y. Yu, C.-X. Li, Z.-Y. He, M.-K. Zhang, M.-D. Liu, Z.-H. Li, J. Feng and X.-Z. Zhang, *Adv. Mater.*, 2018, **30**, 1802006.
29 L. Deng, D. Sheng, M. Liu, L. Yang, H. Ran, P. Li, X. Cai, Y. Sun and Z. Wang, *Biomater. Sci.*, 2020, **8**, 858–870.
30 G. Li, S. Yuan, D. Deng, T. Ou, Y. Li, R. Sun, Q. Lei, X. Wang, W. Shen, Y. Cheng, Z. Liu and S. Wu, *Adv. Funct. Mater.*, 2019, **29**, 1901932.
31 J. Wan, X. Zhang, D. Tang, T. Liu and H. Xiao, *Adv. Mater.*, 2023, **35**, 2209799.
32 C. Wang, Y. Sun, S. Huang, Z. Wei, J. Tan, C. Wu, Q. Chen and X. Zhang, *J. Am. Chem. Soc.*, 2023, **145**, 13099–13113.
33 M. Li, T. Xiong, J. Du, R. Tian, M. Xiao, L. Guo, S. Long, J. Fan, W. Sun, K. Shao, X. Song, J. W. Foley and X. Peng, *J. Am. Chem. Soc.*, 2019, **141**, 2695–2702.
34 J. Zhuang, B. Wang, H. Chen, K. Zhang, N. Li, N. Zhao and B. Z. Tang, *ACS Nano*, 2023, **17**, 9110–9125.
35 D. Cen, Q. Zheng, B. Zheng, R. Zhou, X. Xiao, T. Zhang, Z. Huang, T. Yan, J. Yu, X. Li, R. Deng and X. Cai, *Adv. Funct. Mater.*, 2023, **33**, 2211402.
36 X. Kang, Y. Zhang, J. Song, L. Wang, W. Li, J. Qi and B. Z. Tang, *Nat. Commun.*, 2023, **14**, 5216.
37 W. Wang, C. Zhu, B. Zhang, Y. Feng, Y. Zhang and J. Li, *J. Am. Chem. Soc.*, 2023, **145**, 16642–16649.
38 T. C. Pham, V.-N. Nguyen, Y. Choi, S. Lee and J. Yoon, *Chem. Rev.*, 2021, **121**, 13454–13619.
39 Y. Wan, L.-H. Fu, C. Li, J. Lin and P. Huang, *Adv. Mater.*, 2021, **33**, 2103978.
40 J. Du, T. Shi, S. Long, P. Chen, W. Sun, J. Fan and X. Peng, *Coord. Chem. Rev.*, 2021, **427**, 213604.
41 D. Trachootham, J. Alexandre and P. Huang, *Nat. Rev. Drug Discovery*, 2009, **8**, 579–591.
42 P. Chinna Ayya Swamy, G. Sivaraman, R. N. Priyanka, S. O. Raja, K. Ponnuvel, J. Shanmugpriya and A. Gulyani, *Coord. Chem. Rev.*, 2020, **411**, 213233.
43 R. Song, H. Wang, M. Zhang, Y. Liu, X. Meng, S. Zhai, C.-c. Wang, T. Gong, Y. Wu, X. Jiang and W. Bu, *Angew. Chem., Int. Ed.*, 2020, **59**, 21032–21040.
44 S. Shen, C. Zhu, D. Huo, M. Yang, J. Xue and Y. Xia, *Angew. Chem., Int. Ed.*, 2017, **56**, 8801–8804.
45 J. Sun, X. Cai, C. Wang, K. Du, W. Chen, F. Feng and S. Wang, *J. Am. Chem. Soc.*, 2021, **143**, 868–878.
46 J. Peng, K. Du, J. Sun, X. Yang, X. Wang, X. Zhang, G. Song and F. Feng, *Angew. Chem., Int. Ed.*, 2023, **62**, e202214991.
47 A. Shafferman and G. Stein, *Biochim. Biophys. Acta*, 1977, **462**, 161–170.
48 G. V. Buxton, C. L. Greenstock, W. P. Helman and A. B. Ross, *J. Phys. Chem. Ref. Data*, 1988, **17**, 513–886.
49 J. Geng, Y. Zhang, Q. Gao, K. Neumann, H. Dong, H. Porter, M. Potter, H. Ren, D. Argyle and M. Bradley, *Nat. Chem.*, 2021, **13**, 805–810.
50 J. Zhang, C. Mück-Lichtenfeld and A. Studer, *Nature*, 2023, **619**, 506–513.
51 J. Peng and F. Feng, *Chem.–Eur. J.*, 2024, **30**, e202302842.
52 S. B. Reddy and S. K. Williamson, *Expert Opin. Invest. Drugs*, 2009, **18**, 77–87.

53 Y. Yoshida, N. Itoh, Y. Saito, M. Hayakawa and E. Niki, *Free Radical Res.*, 2004, **38**, 375–384.
54 Y. Wan, G. Lu, J. Zhang, Z. Wang, X. Li, R. Chen, X. Cui, Z. Huang, Y. Xiao, J. Chelora, W. Zhang, Y. Liu, M. Li, H.-Y. Xie and C.-S. Lee, *Adv. Funct. Mater.*, 2019, **29**, 1903436.
55 Y. Liu, P. Tang, P. Xiao, S. Luo, S. Zhang, H. Zhang, Y. Yang and D. Wu, *Adv. Funct. Mater.*, 2022, **32**, 2201666.
56 W. Zhang, H. Zhou, D. Gong, H. Wu, X. Huang, Z. Miao, H. Peng and Z. Zha, *Adv. Healthcare Mater.*, 2023, **12**, 2202947.
57 G. K. Thirunavukkarasu, G. R. Nirmal, H. Lee, M. Lee, I. Park and J. Y. Lee, *J. Ind. Eng. Chem.*, 2019, **69**, 405–413.
58 X. Li, Y. Liu, F. Fu, M. Cheng, Y. Liu, L. Yu, W. Wang, Y. Wan and Z. Yuan, *Nano-Micro Lett.*, 2019, **11**, 68.
59 X. Liu, Y. Yang, M. Ling, R. Sun, M. Zhu, J. Chen, M. Yu, Z. Peng, Z. Yu and X. Liu, *Adv. Funct. Mater.*, 2021, **31**, 2101709.
60 S. Kuang, L. Sun, X. Zhang, X. Liao, T. W. Rees, L. Zeng, Y. Chen, X. Zhang, L. Ji and H. Chao, *Angew. Chem., Int. Ed.*, 2020, **59**, 20697–20703.
61 S. Kuang, F. Wei, J. Karges, L. Ke, K. Xiong, X. Liao, G. Gasser, L. Ji and H. Chao, *J. Am. Chem. Soc.*, 2022, **144**, 4091–4101.
62 E. J. Hong, D. G. Choi and M. S. Shim, *Acta Pharm. Sin. B*, 2016, **6**, 297–307.
63 W. Wu, X. Shao, J. Zhao and M. Wu, *Adv. Sci.*, 2017, **4**, 1700113.
64 W. Jiang, M. Liang, Q. Lei, G. Li and S. Wu, *Cancers*, 2023, **15**, 585.
65 X. Li, S. Kolemen, J. Yoon and E. U. Akkaya, *Adv. Funct. Mater.*, 2017, **27**, 1604053.
66 W. Zhai, Y. Zhang, M. Liu, H. Zhang, J. Zhang and C. Li, *Angew. Chem., Int. Ed.*, 2019, **58**, 16601–16609.
67 J. Sun, X. Zhang, X. Wang, J. Peng, G. Song, Y. Di, F. Feng and S. Wang, *Angew. Chem., Int. Ed.*, 2022, **61**, e202213765.
68 F. Danhier, O. Feron and V. Préat, *J. Controlled Release*, 2010, **148**, 135–146.
69 L. Hui and Y. Chen, *Cancer Lett.*, 2015, **368**, 7–13.
70 J. M. Brown and W. R. Wilson, *Nat. Rev. Cancer*, 2004, **4**, 437–447.
71 R. A. Cairns, I. S. Harris and T. W. Mak, *Nat. Rev. Cancer*, 2011, **11**, 85–95.
72 H.-W. Liu, X.-X. Hu, K. Li, Y. Liu, Q. Rong, L. Zhu, L. Yuan, F.-L. Qu, X.-B. Zhang and W. Tan, *Chem. Sci.*, 2017, **8**, 7689–7695.
73 K. Kiyose, K. Hanaoka, D. Oushiki, T. Nakamura, M. Kajimura, M. Suematsu, H. Nishimatsu, T. Yamane, T. Terai, Y. Hirata and T. Nagano, *J. Am. Chem. Soc.*, 2010, **132**, 15846–15848.
74 R. M. Phillips, *Cancer Chemother. Pharmacol.*, 2016, **77**, 441–457.
75 J. Xiong, P. Wang, S. Son, C. Zhong, F. Zhang, Z. Mao, Z. Liu and J. S. Kim, *Matter*, 2022, **5**, 1502–1519.
76 J. Tian, B. Li, F. Zhang, Z. Yao, W. Song, Y. Tang, Y. Ping and B. Liu, *Angew. Chem., Int. Ed.*, 2023, **62**, e202307288.
77 Z. Liu, F. Song, W. Shi, G. Gurzadyan, H. Yin, B. Song, R. Liang and X. Peng, *ACS Appl. Mater. Interfaces*, 2019, **11**, 15426–15435.
78 F. Xu, H. Li, Q. Yao, H. Ge, J. Fan, W. Sun, J. Wang and X. Peng, *Chem. Sci.*, 2019, **10**, 10586–10594.
79 S. Bhattacharya, B. G. Prajapati and S. Singh, *Crit. Rev. Oncol. Hematol.*, 2023, **185**, 103961.
80 M. Ashrafizadeh, M. Delfi, A. Zarrabi, A. Bigham, E. Sharifi, N. Rabiee, A. C. Paiva-Santos, A. P. Kumar, S. C. Tan, K. Hushmandi, J. Ren, E. N. Zare and P. Makvandi, *J. Controlled Release*, 2022, **351**, 50–80.
81 M. Yang, Z. Özdemir, H. Kim, S. Nah, E. Andris, X. Li, Z. Wimmer and J. Yoon, *Adv. Healthcare Mater.*, 2022, **11**, 2200529.
82 H. Xiong, K. Zhou, Y. Yan, J. B. Miller and D. J. Siegwart, *ACS Appl. Mater. Interfaces*, 2018, **10**, 16335–16343.
83 J. Zhu, Y. Zhang, Z. Li, X. Bao, Y. Zhou, B. Ma, Y. Xie, P. Yan, Z. Wu, Q. Zhang, J. Zou and X. Chen, *Mater. Horiz.*, 2023, **10**, 3014–3023.
84 W. Hu, T. He, H. Zhao, H. Tao, R. Chen, L. Jin, J. Li, Q. Fan, W. Huang, A. Baev and P. N. Prasad, *Angew. Chem., Int. Ed.*, 2019, **58**, 11105–11111.
85 Y. Lu, A. A. Aimetti, R. Langer and Z. Gu, *Nat. Rev. Mater.*, 2016, **2**, 16075.
86 P. Cen, J. Huang, C. Jin, J. Wang, Y. Wei, H. Zhang and M. Tian, *Aggregate*, 2023, **4**, e352.
87 G. B. Bodedla, X. Zhu and W.-Y. Wong, *Aggregate*, 2023, **4**, e330.
88 Y. Hu, S.-Y. Yin, W. Liu, Z. Li, Y. Chen and J. Li, *Aggregate*, 2023, **4**, e256.
89 K. R. Shreder, E. C. K. Lin, J. Wu, J. Cajica, C. M. Amantea, Y. Hu, E. Okerberg, H. E. Brown, L. M. Pham, D. M. Chung, A. S. Fraser, E. McGee, J. S. Rosenblum and J. W. Kozarich, *Bioorg. Med. Chem. Lett.*, 2012, **22**, 5748–5751.
90 X. Yue, B. Wang, M. Lan, J. Fan, X. Song and J. W. Foley, *Chem. Commun.*, 2023, **59**, 4676–4679.
91 Z. Li, S. Li, Y. Guo, C. Yuan, X. Yan and K. S. Schanze, *ACS Nano*, 2021, **15**, 4979–4988.
92 D. Tsvirkun, Y. Ben-Nun, E. Merquiol, I. Zlotver, K. Meir, T. Weiss-Sadan, I. Matok, R. Popovtzer and G. Blum, *J. Am. Chem. Soc.*, 2018, **140**, 12010–12020.
93 T. Weiss-Sadan, Y. Ben-Nun, D. Maimoun, E. Merquiol, I. Abd-Elrahman, I. Gotsman and G. Blum, *Theranostics*, 2019, **9**, 5731–5738.
94 D. Luo, X. Wang, E. Walker, J. Wang, S. Springer, J. Lou, G. Ramamurthy, C. Burda and J. P. Basilion, *ACS Nano*, 2020, **14**, 15193–15203.
95 L. K. B. Tam, J. C. H. Chu, L. He, C. Yang, K.-C. Han, P. C. K. Cheung, D. K. P. Ng and P.-C. Lo, *J. Am. Chem. Soc.*, 2023, **145**, 7361–7375.
96 Z. Ruan, P. Yuan, T. Li, Y. Tian, Q. Cheng and L. Yan, *Eur. J. Pharm. Biopharm.*, 2019, **135**, 25–35.
97 H. Chen, J. Tian, W. He and Z. Guo, *J. Am. Chem. Soc.*, 2015, **137**, 1539–1547.
98 H. Chen, W. He and Z. Guo, *Chem. Commun.*, 2014, **50**, 9714–9717.

99 G. Dai, J. C. H. Chu, C. K. W. Chan, C. H. J. Choi and D. K. P. Ng, *Nanoscale*, 2021, **13**, 15899–15915.
100 G. Wang, Y. Su, X. Chen, Y. Zhou, P. Huang, W. Huang and D. Yan, *Bioact. Mater.*, 2023, **25**, 189–200.
101 Q. Sun, Q. Su, Y. Gao, K. Zhou, W. Song, P. Quan, X. Yang, Z. Ge, Y. Zhang and G. He, *Aggregate*, 2023, **4**, e298.
102 Q. Yang, G. Wu, Y. Yang, Y. Zhou, J. Song, H. Gao and W. Huang, *Adv. Funct. Mater.*, 2024, **34**, 2402194.
103 J. Sun, K. Du, J. Diao, X. Cai, F. Feng and S. Wang, *Angew. Chem., Int. Ed.*, 2020, **59**, 12122–12128.
104 J. Sun, X. Li, J. Cao, Q. Sun, Y. Zhang, X. Wang, T. Wu, X. Hu and F. Feng, *Chem.–Eur. J.*, 2019, **25**, 9164–9169.
105 Y. Li, D. Hu, M. Pan, Y. Qu, B. Chu, J. Liao, X. Zhou, Q. Liu, S. Cheng, Y. Chen, Q. Wei and Z. Qian, *Biomaterials*, 2022, **288**, 121700.
106 Y. Zhang, C. Xu, X. Yang and K. Pu, *Adv. Mater.*, 2020, **32**, 2002661.
107 J. Sun, H. Li, X. Gu and B. Z. Tang, *Adv. Healthcare Mater.*, 2021, **10**, 2101177.
108 A. P. Gorka, R. R. Nani, J. Zhu, S. Mackem and M. J. Schnermann, *J. Am. Chem. Soc.*, 2014, **136**, 14153–14159.
109 J. Liu, H.-J. Butt and S. Wu, *Adv. Funct. Mater.*, 2020, **30**, 1907605.
110 L. Zhang, P. Wang, X.-Q. Zhou, L. Bretin, X. Zeng, Y. Husiev, E. A. Polanco, G. Zhao, L. S. Wijaya, T. Biver, S. E. Le Dévédec, W. Sun and S. Bonnet, *J. Am. Chem. Soc.*, 2023, **145**, 14963–14980.
111 X. Chen, N. Niu, D. Li, Z. Zhang, Z. Zhuang, D. Yan, J. Li, Z. Zhao, D. Wang and B. Z. Tang, *Adv. Funct. Mater.*, 2023, **33**, 2211571.
112 G. He, M. He, R. Wang, X. Li, H. Hu, D. Wang, Z. Wang, Y. Lu, N. Xu, J. Du, J. Fan, X. Peng and W. Sun, *Angew. Chem., Int. Ed.*, 2023, **62**, e202218768.
113 J.-S. Lan, R.-F. Zeng, Z. Li, Y. Wu, L. Liu, L.-X. Chen, Y. Liu, Y.-T. He, T. Zhang and Y. Ding, *ACS Appl. Mater. Interfaces*, 2023, **15**, 34554–34569.
114 H. Wang, J. Chen, Q. Dong, X. Jia, D. Li, J. Wang and E. Wang, *Nano Res.*, 2022, **15**, 5256–5261.
115 A. Chiarugi, C. Dölle, R. Felici and M. Ziegler, *Nat. Rev. Cancer*, 2012, **12**, 741–752.
116 H. Huang, S. Banerjee, K. Qiu, P. Zhang, O. Blacque, T. Malcomson, M. J. Paterson, G. J. Clarkson, M. Staniforth, V. G. Stavros, G. Gasser, H. Chao and P. J. Sadler, *Nat. Chem.*, 2019, **11**, 1041–1048.
117 N. Lu, Z. Deng, J. Gao, C. Liang, H. Xia and P. Zhang, *Nat. Commun.*, 2022, **13**, 2245.
118 Z. Fan, J. Huang, H. Huang and S. Banerjee, *Chemmedchem*, 2021, **16**, 2480–2486.
119 C. Huang, C. Liang, T. Sadhukhan, S. Banerjee, Z. Fan, T. Li, Z. Zhu, P. Zhang, K. Raghavachari and H. Huang, *Angew. Chem., Int. Ed.*, 2021, **60**, 9474–9479.
120 Z. Zhu, L. Wei, Y. Lai, O. W. L. Carter, S. Banerjee, P. J. Sadler and H. Huang, *Dalton Trans.*, 2022, **51**, 10875–10879.
121 E. Zafon, I. Echevarría, S. Barrabés, B. R. Manzano, F. A. Jalón, A. M. Rodríguez, A. Massaguer and G. Espino, *Dalton Trans.*, 2022, **51**, 111–128.
122 D. Hanahan and R. A. Weinberg, *Cell*, 2011, **144**, 646–674.
123 H.-Q. Ju, J.-F. Lin, T. Tian, D. Xie and R.-H. Xu, *Signal Transduction Targeted Ther.*, 2020, **5**, 231.
124 S. Shamjith, M. M. Joseph, V. P. Murali, G. S. Remya, J. B. Nair, C. H. Suresh and K. K. Maiti, *Biosens. Bioelectron.*, 2022, **204**, 114087.
125 F. E. Poynton, S. A. Bright, S. Blasco, D. C. Williams, J. M. Kelly and T. Gunnlaugsson, *Chem. Soc. Rev.*, 2017, **46**, 7706–7756.
126 J. Liu, C. Zhang, T. W. Rees, L. Ke, L. Ji and H. Chao, *Coord. Chem. Rev.*, 2018, **363**, 17–28.
127 S. Monro, K. L. Colón, H. Yin, J. Roque III, P. Konda, S. Gujar, R. P. Thummel, L. Lilge, C. G. Cameron and S. A. McFarland, *Chem. Rev.*, 2019, **119**, 797–828.
128 X. Da, Z. Wang, Y. Jian, C. Zhang, Y. Hou, Y. Yao, X. Wang and Q. Zhou, *Inorg. Chem. Front.*, 2022, **9**, 2544–2556.
129 C. Zhang, J. Huang, X. Guo, X. Da, Z. Dai, M. Hassan, Y. Yu, X. Wang and Q. Zhou, *Nano Today*, 2023, **50**, 101824.
130 N. Tian, W. Sun, X. Guo, J. Lu, C. Li, Y. Hou, X. Wang and Q. Zhou, *Chem. Commun.*, 2019, **55**, 2676–2679.
131 J. Liu, A. W. Prentice, G. J. Clarkson, J. M. Woolley, V. G. Stavros, M. J. Paterson and P. J. Sadler, *Adv. Mater.*, 2023, **35**, 2210363.
132 S. A. E. Omar, P. A. Scattergood, L. K. McKenzie, C. Jones, N. J. Patmore, A. J. H. M. Meijer, J. A. Weinstein, C. R. Rice, H. E. Bryant and P. I. P. Elliott, *Inorg. Chem.*, 2018, **57**, 13201–13212.
133 P. Zhang and H. Huang, *Dalton Trans.*, 2018, **47**, 14841–14854.
134 R. Kushwaha, A. Kumar, S. Saha, S. Bajpai, A. K. Yadav and S. Banerjee, *Chem. Commun.*, 2022, **58**, 4825–4836.
135 C. Ge, J. Zhu, A. Ouyang, N. Lu, Y. Wang, Q. Zhang and P. Zhang, *Inorg. Chem. Front.*, 2020, **7**, 4020–4027.
136 M. Parasram and V. Gevorgyan, *Chem. Soc. Rev.*, 2017, **46**, 6227–6240.
137 Y. M. Wilson, M. Dürrenberger, E. S. Nogueira and T. R. Ward, *J. Am. Chem. Soc.*, 2014, **136**, 8928–8932.
138 Z. Zhu, L. Wei, A. K. Yadav, Z. Fan, A. Kumar, M. Miao, S. Banerjee and H. Huang, *J. Org. Chem.*, 2023, **88**, 626–631.
139 M. Li, Y. Xu, Z. Pu, T. Xiong, H. Huang, S. Long, S. Son, L. Yu, N. Singh, Y. Tong, J. L. Sessler, X. Peng and J. S. Kim, *Proc. Natl. Acad. Sci. U. S. A.*, 2022, **119**, e2210504119.
140 M. Li, K. H. Gebremedhin, D. Ma, Z. Pu, T. Xiong, Y. Xu, J. S. Kim and X. Peng, *J. Am. Chem. Soc.*, 2022, **144**, 163–173.
141 H. Maeda, J. Wu, T. Sawa, Y. Matsumura and K. Hori, *J. Controlled Release*, 2000, **65**, 271–284.
142 M. Ikeda-Imafuku, L. L.-W. Wang, D. Rodrigues, S. Shaha, Z. Zhao and S. Mitragotri, *J. Controlled Release*, 2022, **345**, 512–536.
143 Y. Takakura and Y. Takahashi, *J. Controlled Release*, 2022, **350**, 486–493.
144 Z. Chen, R. K. Kankala, L. Long, S. Xie, A. Chen and L. Zou, *Coord. Chem. Rev.*, 2023, **481**, 215051.

145 G. Szakács, J. K. Paterson, J. A. Ludwig, C. Booth-Genthe and M. M. Gottesman, *Nat. Rev. Drug Discovery*, 2006, **5**, 219–234.
146 A. V. Kabanov, E. V. Batrakova and V. Y. Alakhov, *Adv. Drug Delivery Rev.*, 2002, **54**, 759–779.
147 H. Wang, Z. Gao, X. Liu, P. Agarwal, S. Zhao, D. W. Conroy, G. Ji, J. Yu, C. P. Jaroniec, Z. Liu, X. Lu, X. Li and X. He, *Nat. Commun.*, 2018, **9**, 562.
148 K.-X. Teng, L.-Y. Niu, N. Xie and Q.-Z. Yang, *Nat. Commun.*, 2022, **13**, 6179.
149 J. Karges, *Angew. Chem., Int. Ed.*, 2022, **61**, e202112236.
150 S. A. McFarland, A. Mandel, R. Dumoulin-White and G. Gasser, *Curr. Opin. Chem. Biol.*, 2020, **56**, 23–27.
151 L. Tang, A. Zhang, Z. Zhang, Q. Zhao, J. Li, Y. Mei, Y. Yin and W. Wang, *Cancer Commun.*, 2022, **42**, 141–163.
152 N. L. Miyazaki, A. Furusawa, P. L. Choyke and H. Kobayashi, *Cancers*, 2023, **15**, 5117.
153 T. Iwase, K. Ito, T. Nishimura, K. Miyakawa, A. Ryo, H. Kobayashi and M. Mitsunaga, *Nat. Protoc.*, 2023, **18**, 3390–3412.
154 H. Heng, G. Song, X. Cai, J. Sun, K. Du, X. Zhang, X. Wang, F. Feng and S. Wang, *Angew. Chem., Int. Ed.*, 2022, **61**, e202203444.